ACS OMEGA

http://pubs.acs.org/journal/acsodf

Article

Terminators or Guardians? Design, Synthesis, and Cytotoxicity Profiling of Chalcone-Sulfonamide Hybrids

Shaimaa M. Aboukhatwa,* Peter A. Sidhom, Andrea Angeli, Claudiu T. Supuran,* and Haytham O. Tawfik

Cite This: *ACS Omega* 2023, 8, 7666−7683

Read Online

ACCESS | Metrics & More | Article Recommendations | Supporting Information

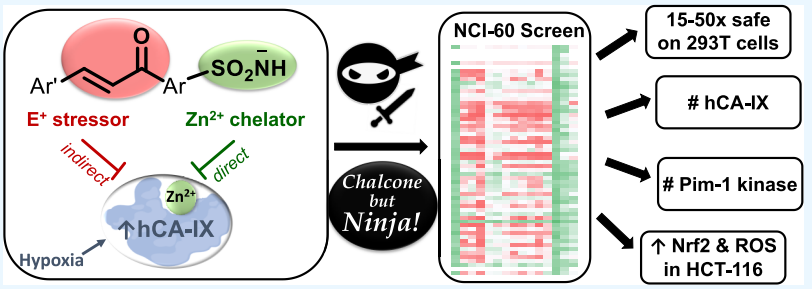

ABSTRACT: With a "less is more" philosophy, a series of 15 chalcone-sulfonamide hybrids were designed anticipating synergistic anticancer activity. The aromatic sulfonamide moiety was included as a known direct inhibitor of carbonic anhydrase IX activity through its zinc chelating property. The chalcone moiety was incorporated as an electrophilic stressor to indirectly inhibit carbonic anhydrase IX cellular activity. Screening by the Developmental Therapeutics Program of the National Cancer Institute, NCI-60, revealed that 12 derivatives were potent inhibitors of cancer cell growth in multiple cell lines and were promoted to the five-dose screen. The cancer cell growth inhibition profile indicated sub- to two-digit micromolar potency (GI_{50} down to 0.3 μM and LC_{50} as low as 4 μM) against colorectal carcinoma cells, in particular. Unexpectedly, most compounds demonstrated low to moderate potency as direct inhibitors of carbonic anhydrase catalytic activity *in vitro,* with **4d** being the most potent, having an average Ki value of 4 μM. Compound **4j** showed ca. six-fold selectivity to carbonic anhydrase IX over the other tested isoforms *in vitro*. Cytotoxicity of both **4d** and **4j** in live HCT116, U251, and LOX IMVI cells under hypoxic conditions confirmed their targeting of carbonic anhydrase activity. Elevation of oxidative cellular stress was stipulated from the increase in Nrf2 and ROS levels in **4j**-treated colorectal carcinoma, HCT116, cells compared to the control. Compound **4j** arrested the cell cycle of HCT116 cells at the G1/S phase. In addition, both **4d** and **4j** showed up to 50-fold cancer cell selectivity compared to the non-cancerous HEK293T cells. Accordingly, this study presents **4d** and **4j** being new, synthetically accessible, simplistically designed derivatives as potential candidates to be further developed as anticancer therapeutics.

HIGHLIGHTS

- Hybrid chalcone-sulfonamides were designed as potential carbonic anhydrase inhibitors.
- The derivatives inhibited cancer cell growth in the NCI-60 screen with high potency.
- Up to 50-fold selectivity on cancer cells compared to normal cells was demonstrated.
- Cell cycle arrest was observed at the G1/S phase in HCT116 colorectal carcinoma cells.
- Nrf2 and ROS levels were elevated in response to one of the compounds in HCT116 cells.

1. INTRODUCTION

Despite their humble arylethenyl ketone structure, chalcones have demonstrated a wide spectrum of biological activities and multiple potential therapeutic applications.[1] A plethora of naturally isolated and nature-inspired synthetic bioactive derivatives encompass a chalcone "privileged" scaffold.[1,2] The literature presents chalcone-based compounds as antioxidant, antimicrobial, antiinflammatory, and antineoplastic agents.[3,4] Several postulated molecular targets for chalcones were reported, including microtubule, protein kinases, oxidoreductases, hydrolases, and retinoic acid receptors, among others.[2,5−7] These "ninja" chalcones are largely undervalued in the drug discovery industry, possibly because of their suspected non-specific reactivity.[8] Only two non-FDA approved, clinically-used

Received: November 13, 2022
Accepted: January 30, 2023
Published: February 17, 2023

chalcone derivatives can be found in the international drug market: metochalcone in the Spanish market, as a choleretic agent, and sofalcone approved in Japan as a gastric mucosal protective agent.[9]

The α,β-unsaturated carbonyl system is recognized as a potential electrophilic Michael acceptor, which contributes to chalcone's reactivity *via* covalently modifying biological nucleophiles (Figure 1).[8] The peril of irreversible promiscuous

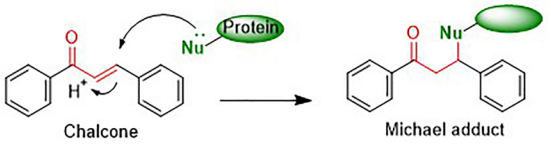

Figure 1. Electrophilic chalcones as Michael acceptors and covalent biological modifiers.

reactivity of such electrophilic structure placed structural alerts on chalcones in some virtual drug screening filters.[10] Nevertheless, these filters are now recognized as being oversensitive and could be eliminating potential good hits for new drug discovery.[11] Considering the recently approved α,β-unsaturated carbonyl- and acrylamide-containing drugs,[12] it has become clear that covalent modifiers, like chalcones, bestow invaluable biological tools and potential therapeutics.[7]

As an example of their targets, chalcones form Michael adducts with the sulfhydryl groups (SH) on the cysteine-rich, redox biosensor, Kelch-like ECH-associated protein 1 (KEAP1), leading to dissociation, nuclear translocation, and activation of the nuclear factor erythroid 2 (NF-E2) p45-related factor 2 (Nrf2).[13] The activated nuclear Nrf2 stimulates the expression of several antioxidant and anti-inflammatory genes. Natural and synthetic compounds possessing chalcone scaffolds were reported as Nrf2 activators.[14] As an example, sofalcone was found to covalently bind to KEAP1 and activate Nrf2, resulting in its anticolitic activity.[15] Although Nrf2 activation is often associated with cytoprotective effects, it was also implicated in the malignant behavior of cancer cells.[16] Within the same context, besides their cytoprotective role, several chalcone derivatives were reported as being cytotoxic.[17] It is hypothesized that being cytoprotective or cytotoxic depends on the particular structure and the dose tested.[6]

On another hand, the activation of oxidative-stress stimulated Nrf2 pathway has been shown to intersect with the hypoxia-induced activation of cancer-related human carbonic anhydrase (hCA) expression.[18] hCA IX is a transmembrane catalytic protein, induced under hypoxia, that has many biological roles, including cell adhesion and invasion.[19] hCA IX is absent from most normal tissues but abundant in several solid tumor tissues: colorectal, breast, bladder, lung, and cervical carcinomas.[20] The high expression level of hCA IX has been linked to pH balance regulation, tumor cell progression, and ultimately, poor outcome in tumorigenesis.[21] In a tissue microarray of surgically resected human hepatocellular carcinomas, active Nrf2 expression was associated with significantly increased hCA IX expression and tumor proliferative activity as well as clinicopathological features.[22]

Additionally, electrophilic Nrf2 activators, which increase oxidative stress and counterbalance the hypoxic media, were reported to have synergistic anticancer activity with hCA inhibitors.[23,24] Particularly, a combination of the Nrf2 activator, sulforaphane,[25] with the gold standard pan hCA inhibitor, acetazolamide, reduced viability of bronchial carcinoid cells, compared to single agents.[23] The same combination of sulforaphane and acetazolamide substantially suppressed viability, growth, and invasiveness of human bladder tumor cell lines *in vitro* and reduced the tumor growth in xenograft-bearing mice *in vivo*.[24] Encouraged by the synergism between hCA inhibitors and electrophilic oxidative stress inducers, we attempted the current molecular design, illustrated in the next section.

2. DESIGN AND SYNTHESIS

2.1. Design Rational. The idea behind the current molecular design is illustrated in Figure 2. The induced activity of hCA IX is an established mechanism that helps cancer cells survive the acidic environment resulting from their high metabolic rate.[26] In addition, solid cancer cells tend to evade apoptosis *via* adopting hypoxic conditions, which induce hCA IX expression (Figure 2).[26] The synergistic anticancer activity of a combination between an electrophile and a carbonic anhydrase inhibitor[23,24] inspired the current molecular design. The hybridization between the sulfonamide and the chalcone moieties was intended to provide dual inhibition of hCA IX activity in cancer cells. The primary aromatic sulfonamide group is a well-established direct inhibitor of carbonic anhydrase catalytic activity.[27] The electrophilic Michael acceptor in the chalcone moiety was expected to induce elevated level of oxidative stress within the cancer cell, which could indirectly inhibit hCA IX activity. Therefore, the chalcone-sulfonamide amalgamate was envisioned beneficial to provide synergism in inhibition of cancer cell growth.

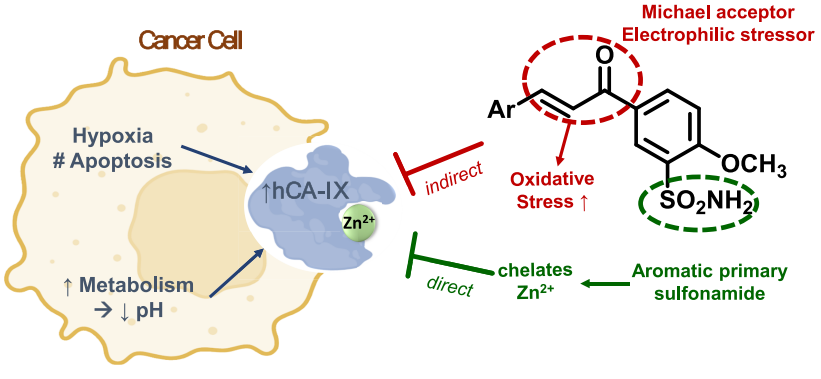

Figure 2. Design rational of chalcone-sulfonamide hybrids to provide synergistic targeting of hCA IX in both a direct and an indirect fashion.

https://doi.org/10.1021/acsomega.2c07285
ACS Omega 2023, 8, 7666−7683

Scheme 1. Synthesis of Chalcone-Sulfonamide Hybrids 4a−4o

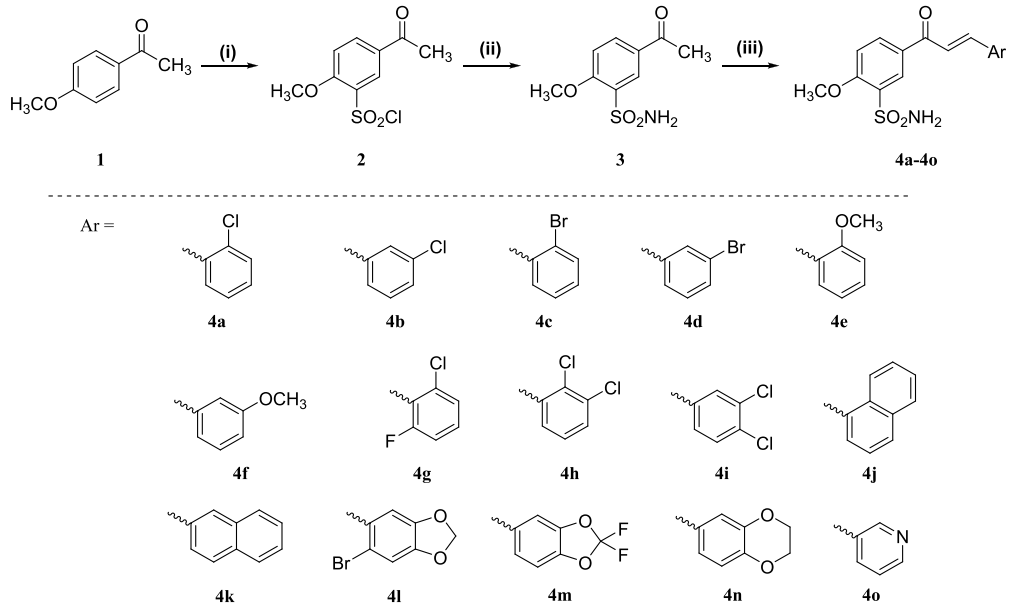

Reagents and Conditions:

(i) $HOSO_2Cl$, $SOCl_2$ at 0 °C-rt, 24 h; **(ii)** EtOH, NH_4OH, rt, 1 h, **(iii)** aldehyde, MeOH:THF (3:7), aq. NaOH, rt, 25 h.

2.2. Chemical Synthesis. The synthetic pathway for the designed derivatives is outlined in Scheme 1 below. The detailed synthetic procedure and chemical characterization are provided in Section 6 and the Supporting information. Briefly, the synthesis started with chlorosulfonation of *p*-methoxyacetophenone **1** using chlorosulfonic acid and excess thionyl chloride to give the sulfonylchloride derivative **2** (Scheme 1). *N*-Sulfonation of ammonia with **2** gave the sulfonamide intermediate **3**. Aldol condensation of **3** with different aromatic aldehydes, of varying Aryl group, yielded chalcone derivatives **4a−4o**.

3. CELL-BASED SCREENING FOR SYNTHETIC COMPOUNDS

3.1. Single-Dose Profiling against a Panel of 60 Cancer Cell Lines by the NCI-60 Screening and Structure−Activity Correlations. The synthesized derivatives **4a−4o** were evaluated for their effect on cancer cell growth in a panel of 60 different cancer cell lines through the Developmental Therapeutics Program (DTP) of the United States National Cancer Institute (NCI).[29,30] The cell lines represented leukemia; non-small cell (NSC) lung cancer; colon cancer; central nervous system (CNS) cancer; melanoma; and ovarian, renal, prostate, and breast cancers. The NCI-60 screen employs the sulphorhodamine B (SRB) assay, which can differentiate cell killing (lethality) from growth inhibition.[31] The initial screening results provided are growth percentages relative to the no-drug control and relative to the number of cells at zero time point. The NCI-DTP one-dose mean graphs are provided in the biological section of the Supporting Information. Values of percentage growth inhibition (% GI) for **4a−4o** were calculated from the values of mean growth percentages as (100 − growth %), and are provided in Table 1. Table entries are highlighted according to the value of % GI with color scales spanning from green (low % GI) to white (median % GI) to red (high % GI). In general, three compounds, **4a**, **4m**, and **4n** resulted in little to no growth inhibition of most cell lines. In some instances, they caused promotion of cellular growth giving a negative % GI (such negative values were omitted in the table for clarity and replaced with a hyphen). Up to 45% growth promoting activity (i.e., % GI down to ca. −45%) was observed in some instances. The other 12 compounds, **4b−4l** and **4o**, had a completely different profile. Most cell lines were overly sensitive to the aforementioned compounds, with % GI values reaching ca. 200% in some cases.

Structure−activity correlation of the compounds to their % GI values indicated that substituents at the arylethenyl group significantly affected the cancer growth inhibition potency (mean % GI) of the derivatives (Table 1 and Figure 3). In general, derivatives with electron-withdrawing substituents (−Cl and −Br) on the arylethenyl phenyl ring were more potent than the ones with the electron-donating group ($-OCH_3$). In other words, the electron density on the arylethenyl group, and hence the electrophilic reactivity of the Michael acceptor, affected the activity (Table 1 and Figure 3).

The reported unsubstituted phenyl derivative **8a** was previously tested in the NCI-60 screen and showed an average % GI of ca. 32%.[28] Replacement of the phenyl in **8a** with a 3-pyridyl group as in **4o**, increased the average % GI to 57% (**Figure 3**). The *para* substitution of the phenyl ring in the arylethenyl group with the electron-donating methoxy in **8d** seemed to have a subtle effect on the potency (**Figure 3**). This can be envisioned from the growth inhibition value for the reported *para*-methoxy derivative (% GI = 21%).[28] The *ortho*- and *meta*-methoxy had a better activity than the *para*-methoxy as seen with % GIs of 76 and 78% for both **4e** and **4f**, respectively (Table 1 and Figure 3).

Ortho-chloro substitution of the arylethenyl phenyl group abolished the activity as in **4a**, with a % GI less than 0, i.e., it had a growth promoting activity. When the chlorine atom moves from the *ortho* position to the *para* position, as in **8b** with a % GI of 56%,[28] the activity rises noticeably. It then rises even more when the chlorine atom moves to the *meta* position, as in **4b** with a % GI of 120% (**Figure 3**).

https://doi.org/10.1021/acsomega.2c07285
ACS Omega 2023, 8, 7666−7683

Table 1. Single-Dose NCI-60 Screening Results and Percent Growth Inhibition of 60 Cancer Cell Lines in Response to 4a−4o[a]

Cell line / compound	Growth Inhibition (%)#														
	4a	4b	4c	4d	4e	4f	4g	4h	4i	4j	4k	4l	4m	4n	4o
Leukemia															
CCRF-CEM	—	93	93	nd*	94	98	94	99	88	95	94	95	—	9	94
HL-60(TB)	nd	nd	nd	nd	nd	nd	nd	nd	nd	nd	nd	nd	—	5	nd
K-562	nd	nd	nd	nd	nd	nd	nd	nd	nd	nd	nd	nd	0	83	nd
MOLT-4	nd	nd	nd	nd	nd	nd	nd	nd	nd	nd	nd	nd	—	63	nd
RPMI-8226	—	105	109	116	96	110	110	109	107	111	117	114	4	41	107
SR	nd	nd	nd	nd	nd	nd	nd	nd	nd	nd	nd	nd	7	82	nd
NSC Lung Cancer															
A549/ATCC	—	182	181	186	94	90	92	103	89	93	178	100	1	52	57
EKVX	3	174	180	168	77	51	91	99	76	106	173	95	—	15	37
HOP-62	—	137	119	187	86	79	98	169	147	82	130	138	—	70	73
HOP-92	—	14	23	110	51	44	90	78	69	27	75	85	—	6	44
NCI–H226	—	62	79	83	60	46	78	81	75	67	80	87	—	—	23
NCI–H23	—	110	121	166	77	85	116	116	124	120	124	131	—	27	78
NCI–H322M	—	89	79	97	70	78	83	88	79	85	89	93	—	15	48
NCI–H460	—	97	99	98	94	84	97	101	93	98	98	100	—	32	90
NCI–H522	—	150	167	179	110	165	161	156	147	167	163	146	—	56	168
Colon Cancer															
COLO 205	—	165	173	193	99	118	185	179	176	179	176	169	—	8	76
HCC-2998	—	99	166	193	71	70	146	149	174	170	177	154	—	1	23
HCT116	—	164	197	199	95	174	190	198	196	192	198	198	—	57	118
HCT15	7	190	191	170	92	107	112	169	138	165	187	140	—	58	95
HT29	—	99	117	156	81	96	92	106	150	140	126	100	—	67	76
KM12	—	158	171	163	93	142	141	162	147	161	174	158	0	14	98
SW-620	—	120	146	120	79	92	95	147	149	116	143	143	—	68	87
CNS Cancer															
SF-268	8	92	86	139	79	61	76	82	75	86	87	82	—	—	56
SF-295	11	189	177	181	78	65	87	138	93	162	180	123	—	21	61
SF-539	3	181	175	196	105	112	163	176	187	183	188	189	—	55	96
SNB-19	3	100	99	143	73	73	80	94	95	90	150	94	7	49	55
SNB-75	—	71	66	117	91	79	70	85	94	49	115	98	—	18	36
U251	—	197	196	198	95	131	187	196	196	194	196	195	1	88	89
Melanoma															
LOX IMVI	—	187	190	192	99	170	169	179	169	184	189	186	—	76	115
MALME-3M	6	72	38	133	50	29	87	77	72	70	82	76	6	12	22
M14	—	111	112	193	91	59	159	177	171	174	178	171	—	10	34
MDA-MB-435	—	86	77	106	73	66	93	86	98	95	98	94	—	12	26
SK-MEL-2	—	19	19	126	22	3	75	26	33	54	47	11	—	—	—
SK-MEL-28	—	126	128	156	61	39	104	119	134	151	142	72	—	—	34
SK-MEL-5	nd	nd	nd	nd	nd	nd	nd	nd	nd	nd	nd	nd	—	0	nd
UACC-257	—	130	84	180	40	34	87	65	98	143	148	36	7	22	28
UACC-62	7	103	66	156	56	47	85	67	104	158	156	61	—	12	25
Ovarian Cancer															
IGROV1	—	93	61	134	61	58	78	90	89	61	108	96	—	36	41
OVCAR-3	9	159	156	148	92	84	163	156	123	151	142	158	—	32	83
OVCAR-4	—	54	65	93	57	42	57	64	65	57	68	72	—	17	8
OVCAR-5	1	118	107	192	88	76	75	108	89	99	143	108	—	—	23
OVCAR-8	—	170	164	195	109	89	97	164	145	114	161	121	—	59	82
NCI/ADR-RES	—	86	84	122	77	87	88	87	85	85	81	86	—	47	31
SK-OV-3	—	50	30	91	53	32	73	57	48	55	77	31	—	1	12
Renal Cancer															
786–0	—	157	178	198	76	85	100	171	194	130	189	140	—	24	50
A498	—	-11	7	7	-5	-15	26	5	-9	-7	3	11	—	—	—
ACHN	—	189	197	195	79	140	114	182	170	127	192	123	—	30	49
CAKI-1	—	110	88	180	79	74	84	106	107	86	98	120	8	14	47
RXF 393	—	166	170	180	101	58	144	171	169	159	160	158	—	11	46
SN12C	3	75	126	179	85	85	87	102	103	93	144	112	—	31	62
TK-10	2	186	97	192	59	79	73	80	95	77	182	83	4	4	33
UO-31	15	168	165	192	75	97	99	181	181	169	187	145	16	51	72
Prostate Cancer															
PC-3	—	68	79	135	52	52	81	95	90	87	112	98	—	—	22
DU-145	—	141	132	137	74	68	100	176	75	87	109	101	—	55	78
Breast Cancer															
MCF7	4	167	171	177	92	92	105	140	149	160	175	102	7	77	93
MDA-MB-231/ATCC	8	104	121	165	93	51	83	98	79	78	94	76	—	13	40
HS 578T	—	5	53	69	40	8	73	64	13	45	31	70	—	13	10
BT-549	nd	nd	nd	nd	nd	nd	nd	nd	nd	nd	nd	nd	—	35	nd
T-47D	—	154	105	171	83	79	106	117	155	103	140	47	—	47	83
MDA-MB-468	—	154	160	154	79	80	104	116	119	156	167	76	—	19	79
Mean % GI	—	120	119	153	76	78	104	119	114	114	134	110	—	29	57

Color Scale: -45 (Minimum) 90 (Median) 200 (Maximum)

[a]Superscript # means that the growth inhibition percentage was calculated as 100 − mean growth percentage. Blank entries (—) indicate no growth inhibition observed, but rather a growth-inducing activity was observed, i.e., a negative value of % GI. The asterisk * means nd = not determined.

The activity increased significantly upon replacing the chloro-substituent with a larger radius bromo-substituent. This can be exemplified by the brominated derivatives **4c** and **4d**, with % GIs of 119 and 153%, respectively, as compared to the chlorinated derivatives **4a** and **4b**, which have % GIs of less than 0 and 120%, respectively. Adding a fluorine substituent to **4a** at the other *ortho* position, the activity increases as can be seen in **4g** with a % GI of 104% (Figure 3).

The presence of another chlorine atom in the *meta* position increases the activity as in a compound **4h** with a % GI of 119%. When the positions of the two chlorine atoms change to become in the *meta* and *para* positions, the activity decreases slightly than if they were in the *meta* and *ortho* positions as in compound **4i** with a % GI of 114% (Table 1 and Figure 3).

The fused bicyclic benzodioxole showed an improved activity upon adding a bromo substituent to the phenyl ring, as seen when comparing **4l** with a % GI of 110% to the previously reported unsubstituted benzodioxole derivative, **8f** with a % GI of 13%.[28] Adding a halogen to the dioxole ring seemed to be deleterious to the activity as seen with the growth promoting activity of **4m** (% GI less than zero). Another fused bicyclic benzodioxane derivative did not show significant change in potency, a % GI of 29%, compared to the phenyl derivative. Both the 1-naphthyl (**4j**) and the 2-naphthyl (**4k**) had average % GIs of 113 and 133%, respectively. (Table 1 and Figure 3).

Compounds that met the NCI-60 screen criteria of significant growth inhibition in a predefined number of cell lines were promoted to testing against the 60-cell panel at five concentration levels.

3.2. Five-Dose NCI-60 Screening of the Selected 12 Derivatives. Twelve compounds, **4b−4l** and **4o**, were advanced to the five-dose screening stage by the NCI, to assess the dose−response curves in the 60-cell line panel. Five 10-fold serial dilutions (100, 10, 1.0, 0.1, and 0.01 μM) for each derivative were tested against each cell line to assess growth percentage following treatment for 48 h. Different parameters were determined from the dose−response relationship: (1) the concentration resulting in 50% growth inhibition, indicated by a 50% reduction in the net protein increase measured by SRB staining in control cells during the drug incubation (GI_{50}); (2) the drug concentration resulting in total growth inhibition (TGI); and (3) the concentration of drug resulting in a 50% net loss of the cells at the end of the drug treatment as compared to that at the beginning (LC_{50}).[29] The values of GI_{50} and LC_{50} for each derivative are summarized in Tables 2 and 3, respectively. The NCI-DTP dose−response curves and other dose response parameters are provided in the Supporting Information.

Examining the GI_{50} values shown in Table 2 indicates that most tested compounds had a GI_{50} less than 5 μM against most cell lines, except for the pyridyl derivative **4o**. The six leukemia cell lines seemed highly susceptible to growth inhibition by all tested derivatives. The growth of chronic myelogenous leukemia cell line, K-562, was inhibited by **4e** and **4l** with GI_{50} values of 0.35 and 0.45 μM, respectively. For the large cell immunoblastic lymphoma SR cell line, derivatives **4b**, **4d**, **4i**, **4j**, and **4k** had a sub-micromolar GI_{50}. Colon cancer cell lines were sensitive to most derivatives, with an average GI_{50} of less than 2 μM, excluding **4o**. All compounds had a low GI_{50} against all colon cancer cell lines. The GI_{50} of most derivatives against the two colorectal carcinoma cell lines, HCT116 and HCT15, was around 1.5 μM, excluding **4o**. A sub-micromolar value for **4i** (GI_{50} = 0.5 μM) and **4k** (GI_{50} = 0.58 μM) was determined against the colorectal adenocarcinoma HCT15 cell line. The

https://doi.org/10.1021/acsomega.2c07285
ACS Omega 2023, 8, 7666−7683

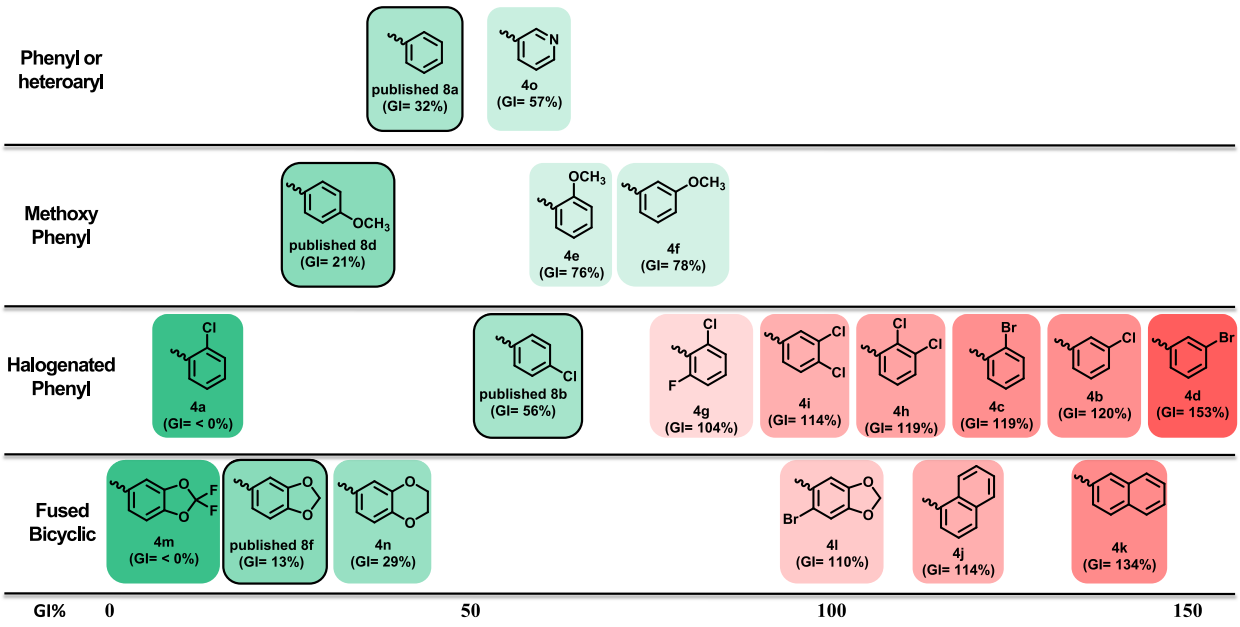

Figure 3. Structure−activity correlation chart for synthesized and reported chalcone-sulfonamide derivatives based on NCI-60 average growth inhibition percentage (% GI).

glioblastoma U251, the melanoma LOX IMVI, and the renal carcinoma UO-31 cells were inhibited with a GI_{50} of around 1.5 μM for most derivatives.

Despite the fact that the tested compounds demonstrated high potency in inhibiting the growth of leukemia cell lines, as indicated by the low values of GI_{50} in Table 2, they were generally not lethal against them (as indicated by the high values of LC_{50} in Table 3). Colon cancer cell lines were killed by most derivatives with a single digit micromolar LC_{50} (<10 μM). Both the 1-naphthyl (**4j**) and the 2-naphthyl (**4k**) had noticeable growth inhibitory activity on colon cancer cell lines, with highest susceptibility of HCT116 cells.

4. MECHANISTIC INVESTIGATIONS AND MOLECULAR TARGET IDENTIFICATION

4.1. *In Vitro* Inhibitory Activity against Human Carbonic Anhydrase Isoforms I, II, IX, and XII. The sulfonamide **3** and the chalcone-sulfonamide hybrids **4a**-**4o** were evaluated for their inhibitory activity against four human carbonic anhydrase (hCA) isoforms of pharmacological relevance; the cytosolic hCA I and hCA II, as well as the transmembrane tumor-associated hCA IX and hCA XII isoforms. Inhibition constants (Ki) of enzyme activity, and the calculated selectivity ratios for **3**, **4c**, **4d**, **4j** and **4l** are presented in Table 4 and Table 5, respectively. The gold standard sulfonamide carbonic anhydrase inhibitor, Acetazolamide, was used as a reference. Representative dose−response curves are provided in the supporting information.

Although the compounds were designed intentionally to directly target hCA activity, through incorporation of a primary sulfonamide moiety, their inhibitory activity was unexpectedly low. Derivatives **4a**, **4b**, **4e**−**4i**, **4k**, and **4m**−**4o** had an inhibition constant (Ki) values greater than the highest tested concentration, 10 μM, against all isoforms. It seems that the methoxy substituent in an *ortho* position to the sulfonamide might be interfering with the hCA-ligand binding.[32]

Given its relatively small structure, sulfonamide **3** was active against the four isoforms with Ki values of 2.32, 4.59, 1.39, and 5.25 μM against hCA I, hCA II, hCA IX, and hCA XII, respectively. Derivative **4c** selectively inhibited hCA IX with a Ki value of 4.71 μM but had no activity on the other tested isoforms. Compound **4d** was the only derivative giving a submicromolar potency with Ki values of 0.85 and 0.50 μM against hCA I and hCA II, respectively, and ca. 10-fold selectivity toward hCA I and hCA II over hCA IX and hCA XII. Compound **4d** had an average Ki value of 4 μM against the four tested isoforms. In terms of selectivity to cancer-related hCA isoforms, **4j** can be regarded as more than six-fold selective to hCA IX over hCA I and hCA II (Table 5).

4.2. *In Vitro* Inhibitory Activity against Pim-1 Kinase. The chalcone moiety is known for inhibition of several targets.[3] Therefore, target prediction analysis through the online SWISS tool was employed to suggest potential other targets for the synthesized derivatives.[33] It predicted a high probability, 40−70%, of targeting several kinases (Supporting Information). Among the predicted kinases was the serine−threonine kinase, Pim-1 kinase. Hence, **4d** and **4j** were tested for inhibitory activity against recombinant Pim-1 kinase *in vitro*. The pan protein kinase inhibitor, staurosporine, was used as a reference. Both **4d** and **4j** were found to be potent inhibitors of Pim-1 kinase activity, with an IC_{50} of ca. 1.06 and 0.34 μM, respectively (Table 6). The naphthyl derivative **4j** was ca. 1.4-fold more potent than the standard kinase inhibitor, staurosporine (IC_{50} = 0.46 μM).

4.3. Non-cancerous Normal Cell Susceptibility to 4d and 4j. Because the derivatives demonstrated a lethal profile against multiple cell lines in the NCI-60 screen, normal cell toxicity was a concern. Therefore, two potent derivatives, **4d** and **4j**, were assessed by a 3-(4,5-dimethylthiazol-2-yl)-2,5-diphenyl-2H-tetrazolium bromide (MTT) assay against the human embryonic kidney cells (HEK293T) as a model of non-cancerous cell lines. The micromolar 50% inhibitory concentration measured in triplicate in the MTT assay andthe standard deviation of measurements ($IC_{50} \pm SD$), determined for each compound, compared with staurosporine as a reference, are shown in Table 7.

https://doi.org/10.1021/acsomega.2c07285
ACS Omega 2023, 8, 7666−7683

Table 2. Five-Dose NCI-60 Screening GI_{50} for Selected Derivatives[a]

Table 2. Five-dose NCI-60 screening GI_{50} for selected derivatives.

	Concentration causing 50 % growth inhibition, GI_{50} (μM)											
	4b	4c	4d	4e	4f	4g	4h	4i	4j	4k	4l	4o
Leukemia												
CCRF-CEM	3.1	3.1	2.5	2.5	2.5	2.6	5.8	2.7	2.5	2.6	6.6	12.6
HL-60(TB)	1.9	2.6	1.6	nd*	1.9	1.7	7.8	1.9	1.4	1.6	nd*	11.0
K-562	2.1	1.9	1.4	0.4	2.1	2.8	2.7	2.0	1.7	1.6	0.5	3.0
MOLT-4	2.4	2.0	2.2	2.4	2.1	2.4	2.1	2.3	2.3	2.1	2.3	3.5
RPMI-8226	2.3	2.3	2.0	2.5	2.5	2.6	2.9	1.7	1.6	1.6	2.9	9.1
SR	0.9	1.5	0.7	1.5	1.3	1.4	1.6	0.8	0.7	0.9	1.6	1.8
NSC Lung Cancer												
A549/ATCC	2.5	2.7	2.8	3.1	2.6	2.4	2.5	2.2	2.6	2.0	2.7	13.8
EKVX	4.2	9.8	5.3	3.6	8.1	4.1	10.2	2.1	3.6	6.6	9.8	11.8
HOP-62	2.2	2.4	2.0	2.9	2.7	3.0	2.3	1.9	2.0	2.0	2.6	15.5
HOP-92	2.3	3.3	1.8	2.1	6.3	3.6	5.5	2.3	2.1	1.9	5.5	nd*
NCI-H226	2.8	2.5	2.8	4.0	2.8	3.2	2.3	3.0	3.1	2.3	2.8	14.5
NCI-H23	1.8	3.2	1.8	2.3	4.7	3.0	3.8	1.7	2.2	1.7	4.3	12.0
NCI-H322M	2.1	3.3	2.2	3.2	3.1	3.1	2.8	2.1	2.6	2.3	3.8	12.3
NCI-H460	3.3	2.0	3.2	2.1	3.5	3.0	1.9	2.8	1.8	3.0	4.0	9.1
NCI-H522	1.6	1.8	1.6	2.1	2.5	1.7	3.0	1.6	1.6	1.6	2.8	10.5
Colon Cancer												
COLO 205	1.8	2.2	1.9	3.6	3.0	2.2	2.8	1.8	1.7	2.0	5.4	13.8
HCC-2998	1.6	2.9	1.5	2.6	2.9	2.8	4.2	1.4	1.7	1.6	5.4	13.8
HCT116	1.2	1.5	1.1	2.5	1.6	1.8	1.3	1.2	1.3	1.9	1.6	3.2
HCT15	1.2	1.7	1.0	2.0	1.3	1.4	1.3	0.5	1.2	0.6	1.8	4.2
HT29	1.7	2.3	1.6	3.1	1.9	1.9	1.5	1.5	1.7	1.7	1.9	5.5
KM12	1.6	1.9	1.4	2.9	2.1	2.6	2.0	0.9	1.5	1.6	2.5	3.8
SW-620	1.7	1.8	1.7	2.9	3.2	3.6	1.6	1.4	1.6	1.8	2.7	6.5
CNS Cancer												
SF-268	3.2	3.6	3.0	3.3	4.9	3.3	3.5	2.9	3.0	3.2	5.4	13.5
SF-295	2.2	4.2	2.1	2.6	2.9	3.1	3.9	1.7	2.4	1.9	6.2	12.9
SF-539	1.7	1.7	1.7	2.2	2.0	2.0	1.4	1.7	1.6	1.7	1.7	4.4
SNB-19	3.2	4.3	2.9	4.0	4.8	4.3	5.1	1.9	3.5	2.1	5.8	13.5
U251	1.4	1.5	1.4	2.6	2.5	1.7	1.3	1.4	1.5	1.2	1.6	7.4
Melanoma												
LOX IMVI	1.3	1.7	1.2	2.0	1.6	1.6	1.4	0.7	1.4	1.3	1.7	4.7
MALME-3M	3.6	10.7	3.2	4.0	12.3	4.0	9.8	2.1	1.8	3.2	11.8	14.1
M14	2.1	6.8	1.8	2.7	4.4	2.6	9.6	1.9	2.0	2.2	9.1	14.5
MDA-MB-435	3.2	7.2	2.0	3.0	4.7	3.4	9.6	2.4	2.2	2.4	13.5	14.5
SK-MEL-2	12.9	14.5	8.7	10.5	14.1	4.0	11.2	5.6	5.0	12.3	14.8	19.5
SK-MEL-28	2.8	8.3	2.1	4.5	9.1	3.6	11.0	1.7	1.9	2.1	14.5	14.8
SK-MEL-5	3.2	7.8	2.3	3.9	5.3	3.1	9.1	2.5	2.5	3.5	9.1	14.8
UACC-257	5.5	12.0	3.2	6.0	10.2	3.0	11.2	2.5	3.0	3.8	14.8	15.9
UACC-62	2.0	3.6	1.7	3.0	4.2	2.0	4.9	1.5	1.5	1.6	4.1	12.9
Ovarian Cancer												
IGROV1	2.5	2.8	2.2	3.1	3.0	2.8	3.2	2.0	2.3	2.1	2.8	12.3
OVCAR-3	1.6	2.1	1.3	2.2	2.9	2.5	1.8	1.2	1.8	1.6	2.6	10.2
OVCAR-4	3.6	3.2	4.1	3.6	4.9	4.2	4.0	1.6	2.9	3.0	3.7	16.2
OVCAR-5	1.9	2.2	1.7	2.2	2.6	3.0	1.9	1.6	1.8	1.7	2.6	11.8
OVCAR-8	2.8	2.6	2.3	2.3	3.0	3.0	2.3	2.0	2.4	2.5	2.9	15.1
NCI/ADR-RES	2.3	2.3	2.2	2.3	2.8	2.8	1.9	2.2	2.2	2.7	2.3	23.4
SK-OV-3	6.2	12.9	4.1	7.2	10.0	5.4	12.3	5.5	3.7	4.9	14.5	16.6
Renal Cancer												
786-0	1.6	1.8	1.6	3.2	2.9	3.0	1.9	1.6	1.9	1.7	3.7	11.2
A498	16.2	11.5	13.8	10.7	14.5	15.9	9.6	8.9	13.2	14.5	15.1	21.9
ACHN	1.7	1.8	1.7	3.4	1.9	2.8	1.8	1.7	1.9	1.8	2.0	13.5
CAKI-1	2.4	4.3	2.3	3.2	4.2	4.1	4.4	1.7	2.4	2.1	4.6	12.6
RXF 393	1.6	1.9	1.6	2.3	3.4	1.7	2.1	1.7	1.6	1.6	2.8	12.3
SN12C	1.6	1.9	1.5	2.8	2.8	2.6	1.8	1.4	1.6	1.6	2.0	7.4
TK-10	2.5	3.3	2.2	3.6	2.8	3.6	5.1	2.0	2.9	2.0	14.5	13.8
UO-31	1.3	1.5	1.3	2.9	2.0	3.0	1.5	1.3	1.5	1.3	2.6	6.0
Prostate Cancer												
PC-3	2.2	4.3	2.0	4.8	5.3	4.7	4.5	1.9	2.3	1.8	6.8	16.6
DU-145	3.6	3.3	3.6	3.2	5.8	3.3	2.9	3.5	2.8	3.3	3.7	11.2
Breast Cancer												
MCF7	2.0	2.9	1.6	2.7	2.9	2.2	3.2	1.1	2.1	1.6	3.8	4.9
MDA-MB-231/ATCC	2.2	2.1	2.5	2.8	3.8	2.9	2.6	2.0	2.4	2.5	2.9	13.5
HS 578T	10.7	8.9	15.9	3.3	15.5	6.5	8.7	6.0	5.3	17.4	20.9	20.9
BT-549	1.7	4.6	1.5	2.6	2.5	2.7	4.7	1.6	1.8	1.6	6.0	12.9
T-47D	2.1	3.6	2.1	3.2	3.0	2.4	4.0	2.0	3.4	1.8	6.0	8.9
MDA-MB-468	1.4	2.6	1.4	2.0	2.0	1.5	3.0	1.5	1.6	1.5	5.0	7.1
Average GI_{50}	2.9	4.0	2.6	3.2	4.3	3.1	4.3	2.1	2.4	2.8	5.5	11.5

Color Scale: 0.3 (Minimum) — 2.5 (Median) — 25 (Maximum)

[a]The * means nd = not determined.

Table 3. Five-Dose NCI-60 Screening Lethal Concentration (LC_{50}) for Selected Derivatives[a]

	Concentration causing 50 % lethal effect, LC_{50} (μM)											
	4b	4c	4d	4e	4f	4g	4h	4i	4j	4k	4l	4o
Leukemia												
CCRF-CEM	100	100	100	100	100	100	87.1	100	100	100	100	87.1
HL-60(TB)	100	95.5	1 mM*	nd#	56.2	100	87.1	100	100	18.2	nd	91.2
K-562	100	100	100	100	100	100	87.1	100	100	100	53.7	91.2
MOLT-4	100	100	21.9	100	100	100	87.1	100	100	100	89.1	89.1
RPMI-8226	100	100	100	100	100	100	87.1	100	100	100	100	87.1
SR	100	100	100	100	100	100	87.1	100	100	100	100	91.2
NSC Lung Cancer												
A549/ATCC	42.7	43.7	43.7	49.0	44.7	46.8	38.0	60.3	40.7	37.2	91.2	83.2
EKVX	43.7	47.9	43.7	38.9	46.8	39.8	42.7	12.0	38.0	45.7	100	49.0
HOP-62	24.5	27.5	24.0	36.3	33.1	35.5	25.7	15.8	22.4	28.8	100	69.2
HOP-92	83.2	41.7	47.9	31.6	47.9	97.7	39.8	30.2	33.9	33.9	67.6	nd
NCI-H226	39.8	32.4	42.7	42.7	39.8	44.7	31.6	74.1	52.5	51.3	100	72.4
NCI-H23	6.9	35.5	6.6	30.9	41.7	35.5	35.5	6.8	19.1	6.3	100	49.0
NCI-H322M	30.2	37.2	30.2	35.5	35.5	36.3	31.6	27.5	30.9	28.8	75.9	46.8
NCI-H460	100	100	100	26.9	100	100	38.9	100	9.8	100	100	91.2
NCI-H522	6.3	9.5	6.5	26.9	32.4	7.4	34.7	6.3	6.3	6.8	100	55.0
Colon Cancer												
COLO 205	6.5	9.1	6.5	42.7	36.3	7.2	32.4	6.5	6.3	8.3	100	64.6
HCC-2998	5.9	35.5	6.2	34.7	34.7	33.1	36.3	5.2	6.0	5.5	74.1	49.0
HCT116	5.2	6.0	4.7	33.1	6.9	8.1	5.6	1 mM	6.5	25.7	1 mM	42.7
HCT15	5.9	7.2	5.6	32.4	8.7	8.5	6.8	4.6	8.3	5.5	8.1	40.7
HT29	6.8	100	6.8	32.4	8.5	7.6	5.9	5.2	100	7.4	7.1	69.2
KM12	8.7	8.5	8.1	33.1	18.6	30.9	17.8	6.2	8.7	7.1	49.0	44.7
SW-620	7.4	9.1	1 mM	40.7	79.4	100	6.9	9.3	7.4	7.2	100	91.2
CNS Cancer												
SF-268	51.3	46.8	55.0	45.7	51.3	100	42.7	50.1	41.7	50.1	100	72.4
SF-295	28.2	39.8	24.0	32.4	35.5	33.1	35.5	8.1	27.5	15.8	81.3	49.0
SF-539	8.1	5.9	7.1	12.6	11.7	8.9	4.8	6.3	5.8	5.9	6.3	38.0
SNB-19	35.5	39.8	34.7	38.9	41.7	38.9	37.2	9.5	37.2	21.4	100	47.9
U251	5.4	5.4	5.4	39.8	40.7	7.8	4.7	6.0	6.0	5.1	1 mM	85.1
Melanoma												
LOX IMVI	5.0	5.5	5.0	18.2	7.4	6.9	4.7	4.4	5.1	5.1	5.9	38.0
MALME-3M	39.8	47.9	39.8	41.7	51.3	43.7	41.7	15.8	9.5	40.7	63.1	51.3
M14	26.9	52.5	15.1	36.3	46.8	43.7	46.8	8.1	25.7	28.8	67.6	58.9
MDA-MB-435	38.9	44.7	28.8	41.7	45.7	100	44.7	26.9	28.2	25.1	100	66.1
SK-MEL-2	53.7	55.0	50.1	47.9	53.7	51.3	43.7	42.7	43.7	52.5	61.7	91.2
SK-MEL-28	30.9	45.7	18.2	39.8	45.7	38.9	43.7	6.0	7.2	15.8	64.6	50.1
SK-MEL-5	35.5	45.7	22.9	38.0	42.7	37.2	40.7	25.7	28.8	37.2	89.1	50.1
UACC-257	44.7	50.1	40.7	46.8	50.1	63.1	45.7	34.7	38.0	41.7	100	66.1
UACC-62	19.5	38.9	8.9	35.5	40.7	25.1	37.2	5.9	5.9	6.9	93.3	47.9
Ovarian Cancer												
IGROV1	32.4	31.6	33.1	38.0	37.2	33.9	34.7	18.6	29.5	22.4	57.5	49.0
OVCAR-3	7.4	12.0	7.8	13.8	33.1	30.2	13.8	5.4	11.7	7.2	31.6	45.7
OVCAR-4	42.7	42.7	51.3	61.7	66.1	100	55.0	5.5	47.9	42.7	100	79.4
OVCAR-5	14.8	21.4	11.0	22.4	33.1	33.9	21.4	6.9	11.5	9.8	100	46.8
OVCAR-8	50.1	30.2	50.1	35.5	53.7	49.0	30.2	29.5	36.3	51.3	100	83.2
NCI/ADR-RES	30.2	100	37.2	28.8	36.3	83.2	51.3	57.5	41.7	100	100	91.2
SK-OV-3	45.7	52.5	41.7	47.9	47.9	43.7	45.7	43.7	42.7	51.3	81.3	57.5
Renal Cancer												
786-0	7.8	7.4	6.8	37.2	35.5	42.7	11.7	6.0	8.1	7.8	100	51.3
A498	57.5	51.3	52.5	47.9	55.0	64.6	41.7	50.1	52.5	55.0	55.0	91.2
ACHN	5.9	6.9	5.8	35.5	7.4	28.2	8.5	5.6	8.1	6.3	8.5	47.9
CAKI-1	30.9	39.8	29.5	36.3	40.7	42.7	36.3	10.0	33.9	23.4	100	49.0
RXF 393	6.2	10.2	6.3	31.6	39.8	15.1	27.5	7.1	6.8	7.1	100	50.1
SN12C	8.5	9.3	8.3	32.4	33.1	32.4	8.3	5.4	9.5	6.8	22.9	41.7
TK-10	33.9	35.5	36.3	36.3	36.3	39.8	38.0	21.9	33.1	29.5	89.1	51.3
UO-31	5.8	6.0	5.6	36.3	31.6	34.7	8.3	5.0	6.9	5.1	44.7	40.7
Prostate Cancer												
PC-3	43.7	49.0	18.6	51.3	45.7	69.2	44.7	20.9	30.2	9.1	100	66.1
DU-145	34.7	33.9	36.3	34.7	42.7	36.3	29.5	35.5	33.1	34.7	38.9	45.7
Breast Cancer												
MCF7	35.5	50.1	25.7	40.7	44.7	41.7	47.9	9.5	41.7	23.4	79.4	50.1
MDA-MB-231/ATCC	20.4	11.5	25.7	26.3	37.2	26.9	25.7	8.5	22.9	26.9	66.1	49.0
HS 578T	100	100	100	100	100	100	87.1	100	100	100	100	91.2
BT-549	11.5	40.7	7.9	28.8	30.9	33.9	38.9	6.8	7.4	6.9	100	50.1
T-47D	39.8	87.1	39.8	53.7	46.8	100	57.5	44.7	53.7	49.0	100	72.4
MDA-MB-468	6.0	42.7	5.9	24.5	29.5	14.8	36.3	6.0	6.3	5.9	95.5	46.8
Average	35.9	43.1	31.6	42.8	45.8	49.7	37.7	29.8	33.6	33.2	77.1	62.3

Color Scale: 4 (Minimum) — 40 (Median) — 100 (Maximum)

[a]The * means that 1 mM is an estimated value that indicates a high value of lethal concentration exceeding the highest tested concentration range. The superscript # means nd = not determined.

Both **4d** and **4j** had higher IC_{50} values than staurosporine against HEK293T cells. The cancer cell susceptibility was achieved at an average concentration GI_{50} of 2.6 μM for **4d** and GI_{50} of 2.4 μM for **4j** (Table 2). Compounds **4d** and **4j** had an IC_{50} of ca. 53 and 20 μM, respectively, against normal HEK293T cells (Table 7). The average cancer cell fold selectivity is estimated to be ca. 20-fold and 9-fold for **4d** and **4j**, respectively.

https://doi.org/10.1021/acsomega.2c07285
ACS Omega 2023, 8, 7666−7683

Table 4. Inhibition Constants (Ki) of 3 and 4a−4o against hCA I, II, IX, and XII Compared to Acetazolamide[a]

Compound	Ki (μM)*			
	hCA I	hCA II	hCA IX	XII
3	2.32	4.59	1.39	5.25
4c	>10	>10	4.71	>10
4d	0.85	0.50	8.53	6.09
4j	>10	>10	1.64	7.87
4l	>10	4.01	8.17	6.06
Acetazolamide	0.25	0.01	0.03	0.01

[a]The * denotes the mean of three replicates, with errors ranging in ± 5−10% of the reported values.

Table 5. Selectivity Ratios for Derivatives 3, 4c, 4d, 4j, and 4l against hCA I, II, IX, and XII[a]

Compound	Selectivity ratio			
	I/IX	II/IX	I/XII	II/XII
3	1.67	3.31	0.44	0.87
4c	>2.12	>2.12	ns*	ns
4d	0.10	0.06	0.14	0.08
4j	>6.09	>6.09	>1.27	>1.27
4l	2.49	0.49	1.22	0.66

* ns = non-selective

[a]The * means ns = non-selective.

Table 6. Inhibitory Activity of 4d and 4j against Pim-1 Kinase

compound	Pim-1 kinase IC_{50} (μM ± SD)
4d	1.06 ± 0.05
4j	0.34 ± 0.02
staurosporine	0.46 ± 0.02

Table 7. Normal HEK293T Cell Susceptibility to 4d and 4j to Assess Cancer Cell Selectivity

compound	IC_{50} (μM ± SD)
4d	52.7 ± 2.03
4j	20.4 ± 0.94
staurosporine	17.8 ± 0.91

Given their high potency against the colorectal carcinoma cells, GI_{50} of 1.1 μM for **4d** and GI_{50} of 1.3 μM for **4j** against HCT116 cells (Table 2), the selectivity against colorectal carcinoma HCT116 cells was estimated to be ca. 50- and 15-fold for **4d** and **4j**, respectively. Those are indicators of an acceptable safety profile for the compounds.

4.4. Hypoxic Cancer Cell Susceptibility to 4d and 4j. The chalcone-sulfonamide derivatives **4d** and **4j** were tested for their cytotoxic potential against the human colorectal carcinoma HCT116, the glioblastoma U251, and the melanoma LOX IMVI cell lines under hypoxic conditions. Results are given in Table 8 as 50% inhibitory concentration in micromolar, measured in triplicate in the MTT assay, with the standard deviation of measurements (IC_{50} ± SD). Both derivatives **4d** and **4j** were cytotoxic with a single to double digit IC_{50} values. The HCT116 cells were most susceptible to both **4d** and **4j** with IC_{50} values of 6.32 and 2.94 μM, respectively. **4j** was more potent against the three cell lines compared to **4d** and to staurosporine (Table 8).

Table 8. Cytotoxicity Expressed as IC_{50} (μM ± SD) of 4d and 4j on Hypoxic HCT116, U251, and LOX IMVI Cells

	HCT116	U251	LOX IMVI
4d	6.32 ± 0.38	14.8 ± 0.61	38.3 ± 1.63
4j	2.94 ± 0.19	4.6 ± 0.26	12.1 ± 0.54
staurosporine	5.72 ± 0.33	11.1 ± 0.51	13.7 ± 0.65

4.5. Cell Cycle Analysis and Apoptosis Behavior of HCT116 Cells with and without 4j. Compound **4j** was further investigated for its influence on cell cycle progression in HCT116 cells (Figure 4). Cell growth in different cell cycle phases (G1, S, and G2/M) was measured by flow cytometry in HCT116 cells treated with the DMSO vehicle control compared to the **4j**-treated cells.[34] Compound **4j** interfered with the normal cell cycle of HCT116 cells by arresting cell growth at the G1/S phase after treatment of HCT116 cells with **4j** for 24 h at a concentration of 2.94 μM. This was demonstrated by a decrease in percentage of cells at the G2/M phase (6%) compared to the DMSO-treated cells (17%). Moreover, **4j**-treated cells showed percentages of cells in both S and G1 phases of 42 and 52%, respectively (Figure 4). Meanwhile, control cells demonstrated 36 and 47% of the cells in S and G1 phases, respectively (Figure 4). Furthermore, compound **4j** induced early and late apoptosis (8.3 and 27.8%, respectively) compared to untreated cells (0.4 and 0.2%, respectively) (Figure 4). The total apoptotic cells were increased by 25-fold in the **4j**-treated cells (39.5%) compared to the control-treated cells (1.6%).

4.6. Electrophilic Stressor (4j) Modulates the Levels of Reactive Oxygen Species (ROS) and the Transcriptional Activity of Nrf2 in HCT116 Cells. The ROS level is associated with survival responses at low doses, whereas prolonged ROS exposure activates apoptosis.[35] The mitochondrial ROS levels were linked to cell survival and autophagy in human colon cell carcinoma.[36] To assess the oxidative stress level in response to the chalcone-sulfonamides, the level of reactive oxygen species and the transcriptional activity of nuclear factor erythroid 2-related factor 2 (Nrf2) were estimated in the colorectal carcinoma HCT116 cells with and without **4j** treatment (Figures 5 and 6).

The effect of **4j** on the redox status of HCT116 cells was assessed using the free radical sensor 2,7-dichlorofluorescin diacetate (H2DCFDA) fluorescence probe (Figure 5). The H2DCFDA is hydrolyzed by intracellular esterases to dichlorofluorescin (DCFH), which accumulates intracellularly. The non-fluorescent DCFH gets oxidized to the fluorescent dichlorofluorescein (DCF) in the presence of ROS. Fluorescence is measured at 485 nm for excitation and 530 nm for emission on a flow cytometer and used as an indicator of the intracellular ROS level. The ROS levels were ca. 50% higher in the case of **4j**-treated cells compared to DMSO-treated cells (Figure 5).

The Nrf2 transcriptional activity was measured by an ELISA-based assay in HCT116 cell nuclei (Figure 6). A standard curve of twofold serial dilutions of Nrf2 (0.15−10 ng/mL) was used to determine the Nrf2 concentration in HCT116 cells with and without **4j** treatment. The concentration of Nrf2 was estimated to be 0.89 ng/mL in DMSO-treated HCT116 control cells and 2.92 ng/mL in **4j**-treated HCT116 cells (Figure 6). The **4j**-treated cells showed ca. 3.3-fold increase in the transcriptionally active nuclear Nrf2 (Figure 6).

The redox-sensitive Nrf2 transcription factor is a basic leucine zipper protein that binds to the antioxidant response element

https://doi.org/10.1021/acsomega.2c07285
ACS Omega 2023, 8, 7666−7683

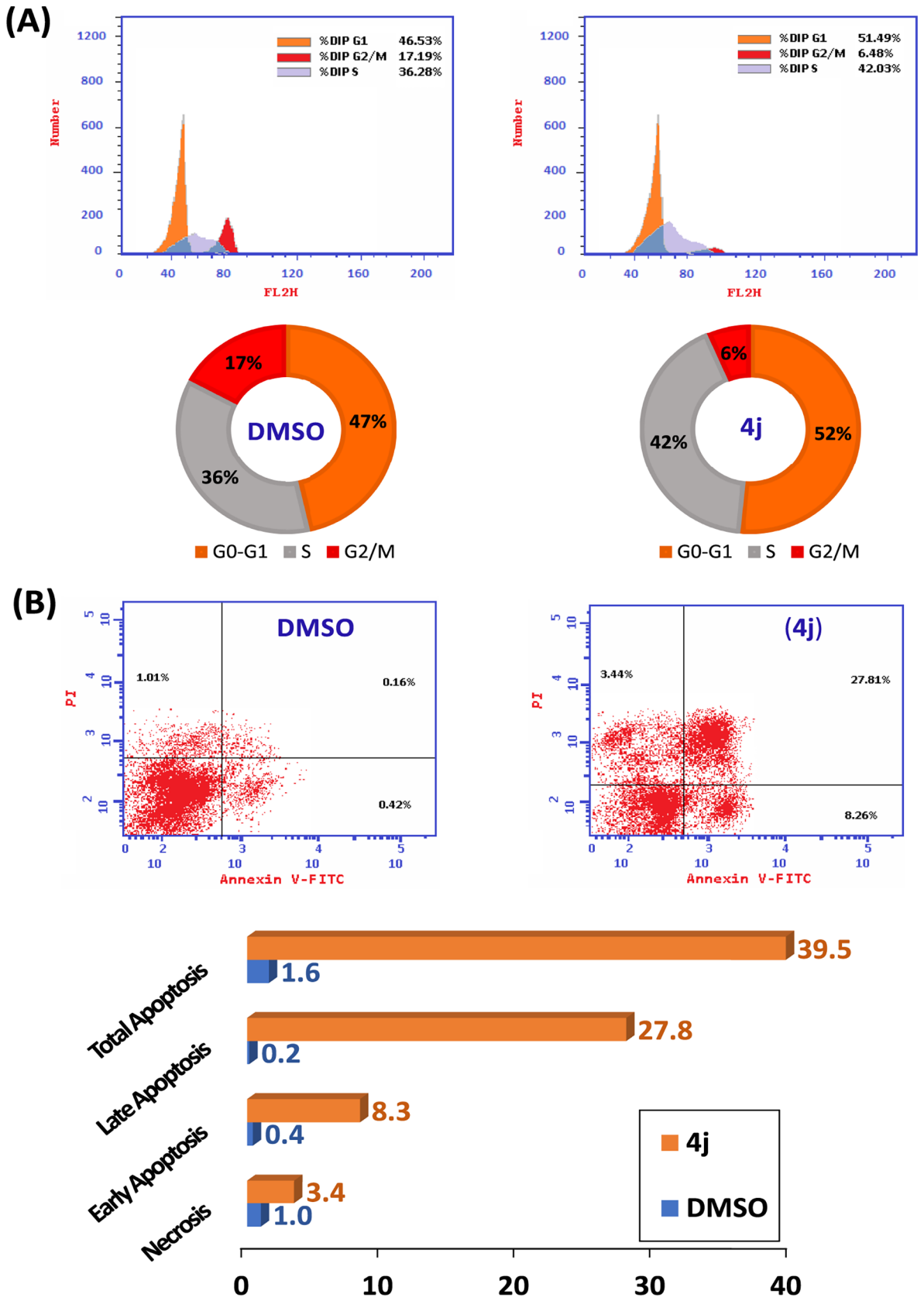

Figure 4. (A) Cell cycle analysis of HCT116 cells treated with the DMSO control and **4j**. (B) Apoptosis effect on the HCT116 cell line stimulated by **4j** compared to the DMSO control. The four quadrants represent LL: viable, LR: early apoptotic, UR: late apoptotic, and UL: necrotic.

and positively regulates the expression of detoxifying enzyme genes.[37] Under normal conditions, Nrf2 is localized in the cytoplasm and is inhibited by KEAP1 and is degraded in the proteasome. In the presence of oxidative and electrophilic

https://doi.org/10.1021/acsomega.2c07285
ACS Omega 2023, 8, 7666−7683

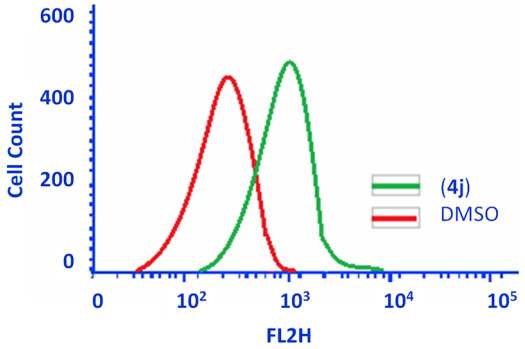

	Fluorescence (AFU)	Fold Change %
(4j)	29026	146.3
Control	19836	100

Figure 5. Flow cytometric histogram of the fluorescence signal height (FL2H) in HDCFDA-stained HCT116 cells, treated with (**4j**) (green line) compared to the DMSO-negative control (red line).

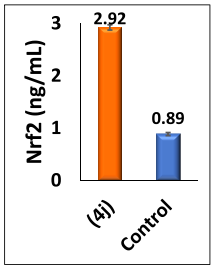

	Nrf2 (ng/mL ± SD)
(4j)	2.92 ± 0.05
Control	0.89 ± 0.03

Figure 6. Nrf2 transcription level measured by ELISA in HCT116 cells with and without (**4j**) treatment.

stressors, the redox-sensitive cysteine residues on KEAP1 are oxidized, resulting in dissociation of KEAP1 from Nrf2.[37] Nrf2 translocates to the nucleus and activates an antioxidant response element-mediated gene expression. Therefore, the transcriptional level of Nrf2 can be used as an indicator of cellular exposure to oxidative or electrophilic stress.[37]

4.7. *In Silico* ADME-Tox Profiling and Docking Simulation. *4.7.1. ADME-Tox Profiling through the SWISS-ADME Online Platform.* The physicochemical properties, human intestinal absorption (HIA), blood−brain barrier (BBB) penetration, drug-likeness, and medicinal chemistry properties of the synthesized compounds were assessed using the online SwissADME online tool.[38] Results are provided in Table 9 and Figure 7.

According to the *in silico* ADME results, all compounds possessed drug-like candidate qualities and did not violate any of the drug-likeness requirements. All compounds are predicted to have high to moderate water solubility, as indicated by the logS value higher than −6. All derivatives are predicted to have high gastrointestinal absorption with an oral bioavailability score of 0.55. All derivatives are drug-like with zero rule violation, according to Lipinski, Ghose, Veber, Muegge, and Egan rules. None of the derivatives gave any alerts in the pan-assay interference compounds (PAINS) filter. One Brenk structural alert[39] for all molecules was returned in calculation, being chalcone with a Michael acceptor property. The polarity estimate, total polar surface area (TPSA) lay between the limit (20−130 Å^2). The lipophilicity estimate, XLOGP3 was in the acceptable range between −0.7 and +5.0. The synthetic accessibility score is less than 3, on a 1−10 scale, implying ease of synthesis.

To predict the passive human gastrointestinal absorption and brain access of our molecules, the BOILED-Egg (Brain Or IntestinaL EstimateD permeation predictive model) plot of WLOGP versus TPSA was retrieved from the Swiss-ADME platform (Figure 8). The BOILED-Egg analysis indicates that all derivatives fell within the permissible range of standard drugs. All derivatives are predicted to fill within the white area of the egg, indicating good human intestinal absorption. None of the derivatives laid in the yellow egg yolk area, which indicate that they do not have BBB permeability, which might limit their efficacy in brain metastases.[40]

Table 9. Physicochemical Descriptors and Predicted ADME Properties of Derivatives 4a−4o[a]

molecule	F-Csp3	HBA	HBD	MR	TPSA	XLOGP3	logS	log Kp	SA
4a	0.06	5	1	88.74	94.84	2.85	−3.87	−6.42	3.02
4b	0.06	5	1	88.74	94.84	2.85	−3.87	−6.42	2.96
4c	0.06	5	1	91.43	94.84	2.92	−4.19	−6.64	3.02
4d	0.06	5	1	91.43	94.84	2.92	−4.19	−6.64	2.99
4e	0.12	6	1	90.23	104.07	2.2	−3.35	−6.86	3.17
4f	0.12	6	1	90.23	104.07	2.2	−3.35	−6.86	3.11
4g	0.06	6	1	88.7	94.84	2.95	−4.03	−6.46	3.05
4h	0.06	5	1	93.75	94.84	3.48	−4.47	−6.19	3.09
4i	0.06	5	1	93.75	94.84	3.48	−4.47	−6.19	2.99
4j	0.05	5	1	101.24	94.84	3.48	−4.44	−6.07	3.15
4k	0.05	5	1	101.24	94.84	3.48	−4.44	−6.07	3.15
4l	0.12	7	1	97.5	113.3	2.73	−4.3	−7.05	3.37
4m	0.12	9	1	89.94	113.3	2.81	−4.07	−6.73	3.31
4n	0.17	7	1	94.6	113.3	1.94	−3.4	−7.21	3.36
4o	0.07	6	1	81.53	107.73	1.16	−2.62	−7.21	2.85

[a]F-Csp3: the fraction of sp^3-hybridized carbon atoms, HBA: the number of hydrogen bond acceptors, HBD: the number of hydrogen bond donors, MR: molar refractivity, TPSA: topological polar surface area, XLOGP3: lipophilicity estimate, logS: solubility estimate, log Kp (cm/s): skin permeation estimate, and SA: synthetic accessibility score for ease of synthesis.

https://doi.org/10.1021/acsomega.2c07285
ACS Omega 2023, 8, 7666−7683

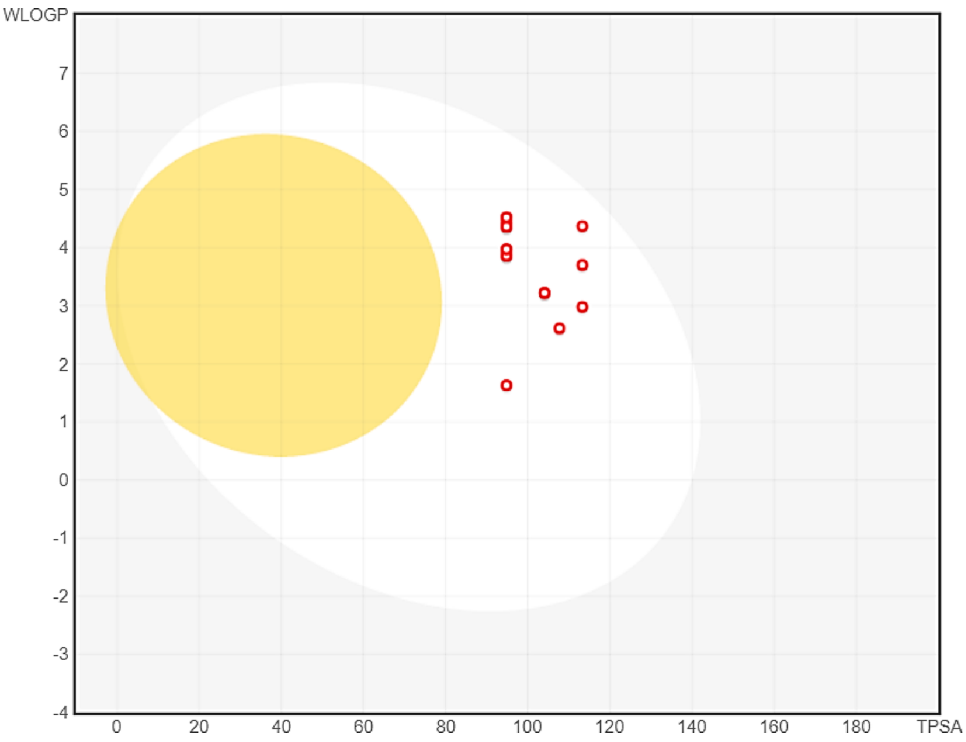

Figure 7. BOILED-Egg representation for the predicted BBB penetration (egg-yolk area), and human intestinal absorption (egg area) of synthesized molecules (small red circles).

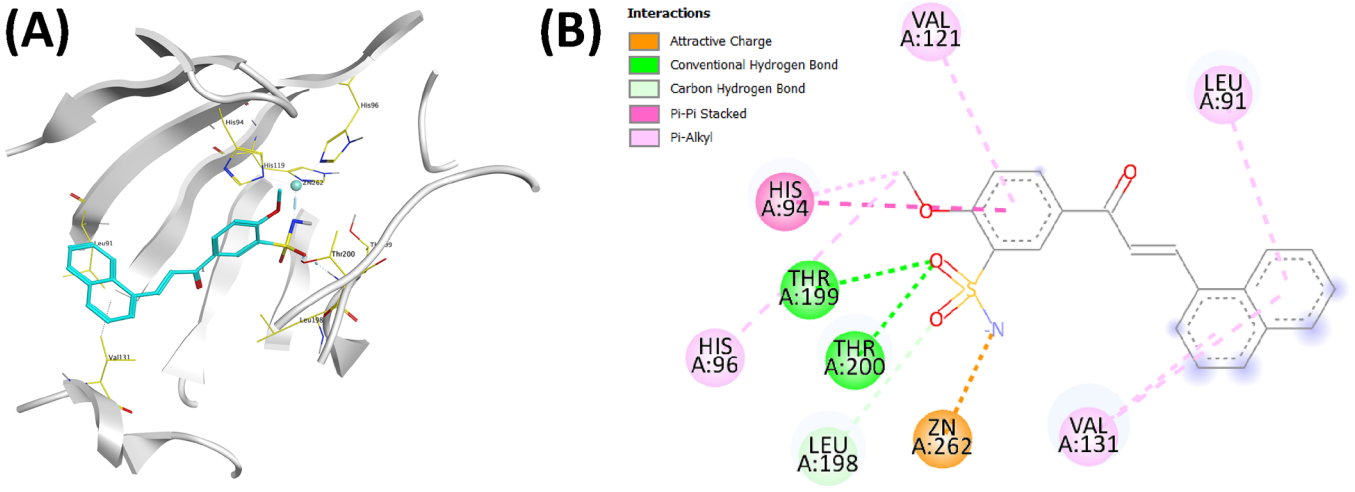

Figure 8. Modeled binding of **4j** with hCA IX (PDB ID: 5FL4). (A) 3D interaction of **4j** with hCA IX. (B) 2D ligand interaction diagram for the **4j** top-scored pose.

*4.7.2. Docking Simulation for the Interaction of **4j** with Carbonic Anhydrase IX.* Docking simulation of **4j** was carried out using the crystal structure of hCA IX, PDB ID: 5FL4,[41] to identify its binding mechanism. The benzenesulfonamide fits tightly into the active site region of hCA IX, as seen by the docking pose of **4j**, with the deprotonated sulfonamide nitrogen, coordinating the active site zinc ion cofactor (Figure 8). According to the docking study into the hCA IX active site, **4j** is predicted to form two hydrogen bonds *via* the S═O of the sulfonamide group with Thr199 and Thr200. The benzenesulfonamide fits into the His94-, His96-, and Val121-defined hydrophobic region (Figure 8). Additionally, it was observed that the naphthalene ring of **4j** interacts hydrophobically with Leu91 and Val131 (Figure 8).

*4.7.3. Docking Simulation for the Interaction of **4j** with Pim-1 Kinase.* Pim-1 kinase is a serine−threonine kinase of 313 amino acids. Non-ATP mimicking inhibitors have been demonstrated to have superior selectivity inhabiting Pim-1 kinase over other kinases.[42] The non-ATP mimetic **4j** was able to form hydrogen bonding interactions, through its sulfonamide group, with hinge region amino acids Asn172 and Asp128 (Figure 9). In addition, the naphthalene ring formed hydrophobic interactions with multiple residues of the unique hydrophobic pocket in the hinge region Leu44, Leu174, and Val126 (Figure 9). The arylethenyl group laid in the hydrophobic tunnel without forming significant interactions (Figure 9).

https://doi.org/10.1021/acsomega.2c07285
ACS Omega 2023, 8, 7666−7683

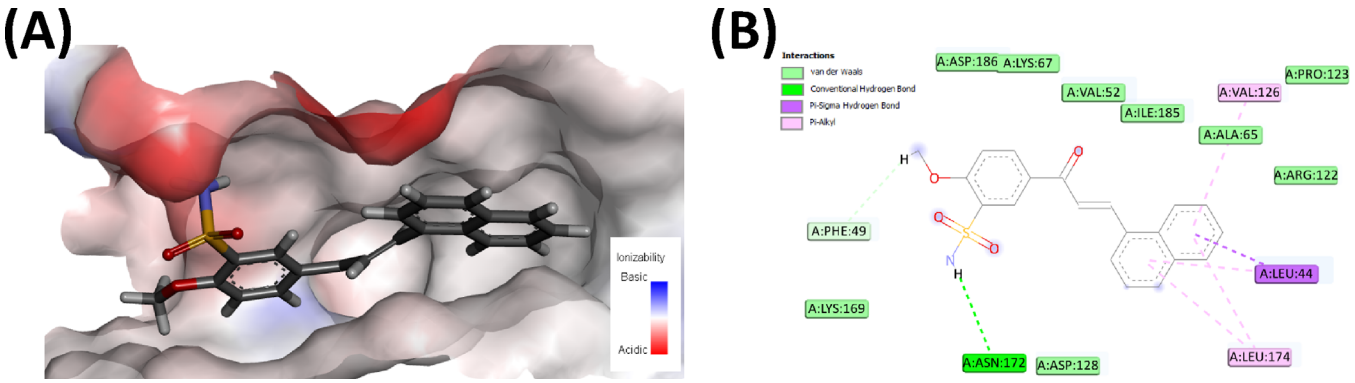

Figure 9. Modeled binding of **4j** with Pim-1 kinase (PDB ID: 2OBJ). (A) 3D interaction of **4j** with Pim-1 kinase active site. (B) 2D ligand interaction diagram for the **4j** top-scored pose in Pim-1 kinase active site.

5. DISCUSSION

In uncontrolled solid tumors, there is insufficient vasculature, especially in the tumor mass center. This reduced tumor blood supply results in a hypoxic microenvironment, leading to upregulation of several transcription factors.[43] The stressful low oxygen level further promotes expression of related genes that help cell survival, metabolism, angiogenesis, and evasion of apoptosis.[44] One of the recently established hypoxia-induced effectors is the transmembrane hCA IX. Generally, hCAs regulate mammalian cellular pH *via* catalyzing the formation of bicarbonate from carbon dioxide.[45] Some hCA isoforms are overexpressed in solid tumor cells, while they are underexpressed in normal ones.[46] hCA IX is overexpressed on the cellular membrane of many solid tumors and is linked to the hypoxic phenotype.[47]

On the hand, the overexpression and aberrant activation of the nuclear Nrf2 was found to promote cell survival and inhibit apoptosis under hypoxic conditions in several cancer types.[48] The peculiar upregulation of Nrf2 has been implicated in solid colorectal tumors and was correlated with poor clinical prognosis and sensitivity to kinase inhibitors.[49] A series of studies investigated the synergism between an hCA inhibitor, acetazolamide, and an Nrf2 activator, sulforaphane.[23,24,50] Acetazolamide is the gold standard pan hCA inhibitor used clinically to treat conditions of excess fluid retention. Sulforaphane is a natural product-derived electrophilic isothiocyanate known to elevate oxidative stress *via* activating the Nrf2.

Taken altogether, the compounds designed in the current study included an aromatic sulfonamide group, a known zinc binding group that inhibits hCA activity. In addition, the conjugated enone containing a scaffold, chalcone, was included to elevate the oxidative stress level in the cancer cell (Figure 2). The amalgamated chalcone-sulfonamides were found to be potent inhibitors of cancer cell growth while being safe on normal cells, indicating specific targeting of the hypoxic cancer cells.

The inhibitory profile of the compounds in the NCI-60 cancer screening (Table 1 and Figure 3) revealed that 12 out of the 15 compounds are highly cytotoxic and were promoted to the five-dose screening (Tables 2 and 3). The other three compounds had no cytotoxic effect, with tumor growth promoting capacity in some cell lines (growth % > 100 i.e. negative % GI). This implies that some most derivatives inhibited the growth of cancer cell "*terminators*", while others maintained or induced cellular growth "*guardians*".

Colorectal carcinoma cell lines were especially sensitive to growth inhibition (Tables 1 and 2) or lethality (Table 3) by most compounds. Colorectal carcinoma is classified among the world's age-standardized top 10 cancers regarding incidence and mortality rates.[51] In 2020, ca. two million new cases were diagnosed with colorectal carcinoma, and ca. one million deaths were reported from colorectal carcinoma.[52] Cytotoxicity of compounds **4d** and **4j** on HCT116, U251, and LOX IMV cells under hypoxic conditions confirms that they could target carbonic anhydrase activity (Table 7). The low cytotoxicity of **4d** and **4j** on HEK293T cells, a non-cancerous cellular model, indicated a high, up to 50-fold, selectivity on cancer cells compared to normal cells (Table 8).

Compound **4j** was found to early interfere with the HCT116 cell cycle, arresting cell growth in the G1/S phase (Figure 4). The ability of the compounds to induce oxidative stress was assessed for derivative **4j** in the colorectal carcinoma HCT116 cells. Both ROS and Nrf2 levels were used as endpoint surrogates of the interference of **4j** with cellular hypoxia as a mechanism leading to its cancer cell lethality (Figures 5 and 6).

The hCA inhibitory activity *in vitro* was unexpectedly low for most derivatives (Table 4), with only **4j** showing greater than six-fold selectivity to cancer-related hCA IX over other tested hCA isoforms (Table 5). The *in vitro* inhibition data of hCA activity could not provide a standalone explanation of the cellular behavior of the compounds. The high growth inhibition and lethality could not be attributed solely to the *in vitro* hCA inhibition. Therefore, kinase inhibitory activity of derivatives **4d** and **4j** on Pim-1 kinase was assessed in an *in vitro* assay (Table 6). The activity of both compounds was either comparable to or higher than the standard reference compound. The *in vitro* inhibitory activity of the compounds against hCA IX and Pim-1 kinase was further studied through docking simulation of **4j** with both enzymes (Figures 8 and 9).

The drug-like properties and medicinal chemistry-relevant physicochemical criteria indicated favorable pharmacokinetic profiles for the compounds, with good intestinal absorption. However, none of the derivatives is predicted to permeate the brain, which could be limiting for applicability to CNS cancers or CNS metastasized cancers. The only alert was returned in containing a conjugated enone, which may be an asset as long as the safety profile for the compounds is adequately assessed.

6. CONCLUSIONS

Following the philosophy of "*less is more*", a series of 15 hybrid molecules were designed. The molecules incorporated a primary

https://doi.org/10.1021/acsomega.2c07285
ACS Omega 2023, 8, 7666−7683

aromatic sulfonamide group, to target hCA activity, and a chalcone part as an oxidative stress elevating moiety. The amalgamated molecules showed high potency against cancer cells in the NCI-60 screen with a good safety profile against normal cells. The hCA inhibitory activity, kinase inhibitory activity, oxidative stress induction, and Nrf2 activation confirmed the multimodal action of the compounds. The study ended with simply designed, easily accessible, relatively potent, and safe anticancer derivatives. Our compounds introduce a good starting point for drug discovery of novel colorectal carcinoma treatments. Future studies will assess their *in vivo* efficacy and safety in animal models.

7. METHODOLOGY

7.1. Chemical Synthesis and Characterization. All reagents and solvents were purchased from commercial resources and were used without further purification, unless mentioned otherwise. Analytical thin layer chromatography (TLC) was used to monitor the reaction progress on 0.2 mm silica gel precoated aluminum sheets (Supelco Co., Silica 60 F_{254}) using *n*-hexane/ethyl acetate (1:9) as an eluent. TLC was visualized by a UV lamp at a 254 nm wavelength. Melting points were determined in open-end glass capillaries using a Stuart SMP30 apparatus and were uncorrected. ^{1}H NMR and ^{13}C NMR spectra were recorded using Bruker spectrometers at 400 and 101 MHz, respectively, at the Faculty of Pharmacy, Mansoura University, Mansoura, Egypt. Tetramethylsilane was used as an internal reference standard in NMR measurements. Chemical shifts were recorded in ppm on the δ scale using DMSO-d_6 as a solvent. Coupling constant values (*J*s) were estimated in Hertz (*Hz*). Splitting patterns were designated as s, singlet; d, doublet; ds, doublet of singlet; dd, doublet of doublet; and m, multiplet. Electron ionization mass spectra (EI-MS) were measured on Thermo Scientific ISQ Single Quadruple MS using a 70 eV ionization energy and helium gas as the carrier gas at a constant 1 mL/min flow rate. Microanalysis was performed for C, H, N, and S on PerkinElmer 2400, and elemental percentages were within ±0.4% of the theoretical values. Both EI-MS and elemental microanalysis were performed at the regional center for mycology and biotechnology, Al-Azhar University, Nasr City, Cairo, Egypt.

7.1.1. Synthesis of Benzenesulfonyl Chloride ***2****.* This step was adopted with necessary optimization of the reaction conditions from the previous literature.[28] During a 30 min ice bath stir, 50 mmol chlorosulfonic acid and 17 mmol thionyl chloride were combined. The reaction mixture was then agitated at room temperature for 24 h while 4-methoxyacetophenone **1** (8.5 mmol) was added in small amounts. It was then chilled in ice water, the resulting precipitate was filtered, and compound **2** was produced by washing the filtrate in water. No additional purification of the product was necessary. An off-white solid; 85% yield; m.p.: 107−108 °C (lit.: 104−105 °C[28]).

7.1.2. Synthesis of Sulfonamide ***3****.* This step was adopted with necessary optimization of the reaction conditions from the previous literature.[28] Compound **2** (0.33 mmol), ammonia (1 mL), and ethanol (1 mL) were mixed and agitated at room temperature for 1 h and checked by TLC. The formed solid was filtered and washed with ethanol and then water. Compound **3** did not need further purification. Compound **3** was obtained as a pale pink solid; 80% yield; m.p.: 202−203 °C (lit.: 195−198 °C[28]).

*7.1.3. General Procedure for Synthesis of the Chalcone-Sulfonamide Hybrids (****4a−4o****).* To a mixture of 5-acetyl-2-methoxybenzene-1-sulfonamide **3** (115 mg, 0.5 mmol) and different aldehydes (0.6 mmol) in a mixture of absolute methanol and THF (3:7) (4 mL) was added an aq. solution of NaOH (50 mg in 1 mL of dist. water). The reaction mixture was stirred at room temperature for 25 h. Then, it was poured into water and neutralized by adding 10% HCl aqueous solution. The powder was formed, filtered, and washed with diethyl ether to afford **4a−4o**.

*7.1.3.1. 5-[(2E)-3-(2-Chlorophenyl)prop-2-enoyl]-2-methoxybenzene-1-sulfonamide (****4a****).* White powder; 85% yield; m.p.: 224−225 °C. ^{1}H NMR (400 MHz, DMSO-d_6) δ ppm: 4.05 (s, 3H, 4-OCH_3 of benzene sulfonamide ring), 7.32 (s, 2H, SO_2NH_2), 7.39 (d, 1H, *J* = 8.0, 3-H of benzene sulfonamide ring), 7.47−7.52 (m, 2H, 4,5-H_2 of chlorophenyl ring), 7.60 (d, 1H, *J* = 16.0, COCH═C**H**), 8.04 (d, 1H, *J* = 8.0, 6-H of chlorophenyl ring), 8.07 (d, 1H, *J* = 16.0, COC**H**═CH), 8.24 (d, 1H, *J* = 8.0, 3-H of chlorophenyl ring), 8.47 (s, 1H, 6-H of benzene sulfonamide ring), 8.53 (d, 1H, *J* = 8.0, 4-H of benzene sulfonamide ring). ^{13}C NMR (101 MHz, DMSO-d_6) δ ppm: 57.28, 113.17, 124.75, 127.41, 128.21, 128.79, 129.13, 129.52, 130.54, 132.29, 132.69, 134.86, 135.44, 139.04, 160.35, and 187.18. MS (ESI) (*m*/*z*): 351.23 $[M + 1]^+$, 353.69 $[M + 3]^+$. Anal. calcd. for $C_{16}H_{14}ClNO_4S$: C, 54.63; H, 4.01; N, 3.98; S, 9.11. Found: C, 54.79; H, 4.23; N, 4.19; S, 9.20.

*7.1.3.2. 5-[(2E)-3-(3-Chlorophenyl)prop-2-enoyl]-2-methoxybenzene-1-sulfonamide (****4b****).* Pale yellow crystals; 81% yield; m.p.: 230−231 °C. ^{1}H NMR (400 MHz, DMSO-d_6) δ ppm: 4.05 (s, 3H, 4-OCH_3 of benzene sulfonamide ring), 7.31 (s, 2H, SO_2NH_2), 7.38 (d, 1H, *J* = 8.0, 3-H of benzene sulfonamide ring), 7.49−7.52 (m, 2H, 4,5-H_2 of chlorophenyl ring), 7.75 (d, 1H, *J* = 16.0, COCH═C**H**), 7.86 (d, 1H, *J* = 8.0, 6-H of chlorophenyl ring), 8.06 (d, 1H, *J* = 16.0, COC**H**═CH), 8.11 (s, 1H, 2-H of chlorophenyl ring), 8.46 (s, 1H, 6-H of benzene sulfonamide ring), 8.55 (d, 1H, *J* = 8.0, 4-H of benzene sulfonamide ring). ^{13}C NMR (101 MHz, DMSO-d_6) δ ppm: 57.26, 113.07, 123.56, 128.42, 128.51, 128.75, 129.67, 130.68, 131.20, 132.32, 134.28, 135.43, 137.39, 142.83, 160.28, and 187.26. MS (ESI) (*m*/*z*): 351.30 $[M + 1]^+$, 353.29 $[M + 3]^+$. Anal. calcd. for $C_{16}H_{14}ClNO_4S$: C, 54.63; H, 4.01; N, 3.98; S, 9.11. Found: C, 54.75; H, 4.20; N, 4.23; S, 9.23.

*7.1.3.3. 5-[(2E)-3-(2-Bromophenyl)prop-2-enoyl]-2-methoxybenzene-1-sulfonamide (****4c****).* Yellow crystals; 50% yield; m.p.: 230−231 °C. ^{1}H NMR (400 MHz, DMSO-d_6) δ ppm: 4.09 (s, 3H, 4-OCH_3 of benzene sulfonamide ring), 7.34−7.58 (m, 5H, SO_2NH_2 + 3-H of benzene sulfonamide ring + 2H, 4,5-H_2 of bromophenyl ring), 7.74−7.83 (m, 1H, COCH═C**H**), 7.99−8.12 (m, 2H, 6-H of bromophenyl ring + COC**H**═CH), 8.22−8.29 (m, 1H, 3-H of bromophenyl ring), 8.49−8.60 (m, 2H, 4,6-H_2 of benzene sulfonamide ring). ^{13}C NMR (101 MHz, DMSO-d_6) δ ppm: 57.25, 113.17, 124.75, 125.85, 128.77 (2C), 129.19, 129.47, 132.12, 132.76, 133.79, 134.28, 135.46, 141.89, 160.33 and 187.25. MS (ESI) (*m*/*z*): 394.98 $[M + 1]^+$, 397.48 $[M + 3]^+$. Anal. calcd. for $C_{16}H_{14}BrNO_4S$: C, 48.50; H, 3.56; N, 3.53; S, 8.09. Found: C, 48.72; H, 3.71; N, 3.77; S, 8.20.

*7.1.3.4. 5-[(2E)-3-(3-Bromophenyl)prop-2-enoyl]-2-methoxybenzene-1-sulfonamide (****4d****).* White crystals; 80% yield; m.p.: 248−250 °C. ^{1}H NMR (400 MHz, DMSO-d_6) δ ppm: 4.05 (s, 3H, 4-OCH_3 of benzene sulfonamide ring), 7.32 (s, 2H, SO_2NH_2), 7.38 (d, 1H, *J* = 8.0, 3-H of benzene sulfonamide ring), 7.43 (t, 1H, *J* = 8.0, 5-H of bromophenyl ring), 7.65 (d, 1H, *J* = 8.0, 4-H of bromophenyl ring), 7.73 (d, 1H, *J* = 16.0, COCH═C**H**), 7.88 (d, 1H, *J* = 8.0, 6-H of bromophenyl ring), 8.04 (d, 1H, *J* = 16.0, COC**H**═CH), 8.22

https://doi.org/10.1021/acsomega.2c07285
ACS Omega 2023, 8, 7666−7683

(s, 1H, 2-H of bromophenyl ring), 8.46 (ds, 1H, J = 4.0, 6-H of benzene sulfonamide ring), 8.55 (dd, 1H, J = 4.0, J = 8.0, 4-H of benzene sulfonamide ring). ^{13}C NMR (101 MHz, DMSO-d_6) δ ppm: 57.23, 113.08, 122.86, 128.65, 128.71, 129.59, 131.32, 131.50, 131.89, 132.10, 133.62, 135.48, 137.50, 142.83, 160.26 and 187.36. MS (ESI) (m/z): 394.88 $[M + 1]^+$, 396.98 $[M + 3]^+$. Anal. calcd. for $C_{16}H_{14}BrNO_4S$: C, 48.50; H, 3.56; N, 3.53; S, 8.09. Found: C, 48.69; H, 3.75; N, 3.79; S, 8.17.

*7.1.3.5. 2-Methoxy-5-[(2E)-3-(2-methoxyphenyl)prop-2-enoyl]benzene-1-sulfonamide (**4e**).* Yellow crystals; 87% yield; m.p.: 208−210 °C. ^{1}H NMR (400 MHz, DMSO-d_6) δ ppm: 3.92 (s, 3H, 4-OCH_3 of methoxyphenyl ring), 4.04 (s, 3H, 4-OCH_3 of benzene sulfonamide ring), 7.06 (t, 1H, J = 8.0, 5-H of methoxyphenyl ring), 7.13 (d, 1H, J = 8.0, 3-H of benzene sulfonamide ring), 7.32 (s, 2H, SO_2NH_2), 7.38 (d, 1H, J = 8.0, 3-H of methoxyphenyl ring), 7.47 (t, 1H, J = 8.0, 4-H of methoxyphenyl ring), 7.92 (d, 1H, J = 16.0, COCH═C**H**), 7.99 (d, 1H, 6-H of methoxyphenyl ring), 8.08 (d, 1H, J = 16.0, COC**H**═CH), 8.45−47 (m, 2H, 4,6-H_2 of benzene sulfonamide ring). ^{13}C NMR (101 MHz, DMSO-d_6) δ ppm: 56.20, 57.20, 112.28, 113.13, 121.21, 121.71, 123.30, 128.63, 129.13, 129.93, 132.14, 132.92, 135.09, 139.15, 158.78, 160.08, and 187.44. MS (ESI) (m/z): 347.36 $[M^+]$. Anal. calcd. for $C_{17}H_{17}NO_5S$: C, 58.78; H, 4.93; N, 4.03; S, 9.23. Found: C, 58.95; H, 5.02; N, 4.20; S, 9.40.

*7.1.3.6. 3-Methoxy-5-[(2E)-3-(2-methoxyphenyl)prop-2-enoyl]benzene-1-sulfonamide (**4f**).* Yellow crystals; 88% yield; m.p.: 198−199 °C. ^{1}H NMR (400 MHz, DMSO-d_6) δ ppm: 3.84 (s, 3H, 4-OCH_3 of methoxyphenyl ring), 4.05 (s, 3H, 4-OCH_3 of benzene sulfonamide ring), 7.05 (d, 1H, J = 8.0, 3-H of benzene sulfonamide ring), 7.34 (s, 2H, SO_2NH_2), 7.36−7.41 (m, 2H, 3,5-H_2 of methoxyphenyl ring), 7.46−7.50 (m, 2H, 4,6-H_2 of methoxyphenyl ring), 7.76 (d, 1H, J = 12.0, COCH═C**H**), 8.08 (d, 1H, J = 12.0, COC**H**═CH), 8.48 (ds, 1H, J = 4.0, 6-H of benzene sulfonamide ring), 8.52 (dd, 1H, , J = 4.0, J = 8.0, 4-H of benzene sulfonamide ring). ^{13}C NMR (101 MHz, DMSO-d_6) δ ppm: 55.70, 57.17, 113.07, 113.93, 117.17, 121.96, 122.09, 128.64, 129.70, 130.55, 131.89, 135.36, 136.32, 144.66160.05, 160.14, and 187.60. MS (ESI) (m/z): 347.18 $[M^+]$. Anal. calcd. for $C_{17}H_{17}NO_5S$: C, 58.78; H, 4.93; N, 4.03; S, 9.23. Found: C, 58.89; H, 5.17; N, 4.24; S, 9.37.

*7.1.3.7. 5-[(2E)-3-(2-Chloro-6-fluorophenyl)prop-2-enoyl]-2-methoxybenzene-1-sulfonamide (**4g**).* White crystals; 90% yield; m.p.: 194−195 °C. ^{1}H NMR (400 MHz, DMSO-d_6) δ ppm: 4.04 (s, 3H, 4-OCH_3 of benzene sulfonamide ring), 7.21 (t, 1H, J = 8.0, 4-H of dihalophenyl ring), 7.34 (s, 2H, SO_2NH_2), 7.39−7.57 (m, 3H, 3-H of benzene sulfonamide ring + 3,5-H_2 of dihalophenyl ring), 7.85 (d, 1H, J = 16.0, COCH═C**H**), 8.03 (d, 1H, J = 16.0, COC**H**═CH), 8.31 (dd, 1H, J = 4.0, J = 8.0, 4-H of benzene sulfonamide ring), 8.42 (ds, 1H, J = 4.0, 6-H of benzene sulfonamide ring). ^{13}C NMR (101 MHz, DMSO-d_6) δ ppm: 57.21, 113.46, 116.16, 121.17, 122.63, 126.92, 128.67, 128.74, 129.66, 132.04, 132.14, 133.73, 135.18, 160.23, 160.45, and 187.35. MS (ESI) (m/z): 370.64 $[M + 1]^+$, 372.31 $[M + 3]^+$. Anal. calcd. for $C_{16}H_{13}ClFNO_4S$: C, 51.97; H, 3.54; N, 3.79; S, 8.67. Found: C, 52.18; H, 3.71; N, 4.02; S, 8.68.

*7.1.3.8. 5-[(2E)-3-(2,3-Dichlorophenyl)prop-2-enoyl]-2-methoxybenzene-1-sulfonamide (**4h**).* White powder; 77% yield; m.p.: 230−231 °C. ^{1}H NMR (400 MHz, DMSO-d_6) δ ppm: 4.05 (s, 3H, 4-OCH_3 of benzene sulfonamide ring), 7.32 (s, 2H, SO_2NH_2), 7.40 (d, 1H, J = 8.0, 3-H of benzene sulfonamide ring), 7.51 (t, 1H, 5-H of dihalophenyl ring), 7.77 (d, 1H, J = 8.0, COCH═C**H**), 8.05 (s, 2H, 4,6-H_2 of dihalophenyl ring), 8.21 (d, 1H, J = 16.0, COC**H**═CH), 8.47 (s, 1H, 6-H of benzene sulfonamide ring), 8.53 (d, 1H, J = 8.0, 4-H of benzene sulfonamide ring). ^{13}C NMR (101 MHz, DMSO-d_6) δ ppm: 57.26, 113.20, 126.12, 127.75, 128.43, 128.99, 129.27, 130.58, 132.53, 133.04, 135.19, 135.54, 137.41, 138.96, 160.44, and 187.14. MS (ESI) (m/z): 384.20 $[M + 1]^+$, 386.66 $[M + 3]^+$. Anal. calcd. for $C_{16}H_{13}Cl_2NO_4S$: C, 49.76; H, 3.39; N, 3.63; S, 8.30. Found: C, 49.92; H, 3.61; N, 3.79; S, 8.37.

*7.1.3.9. 5-[(2E)-3-(3,4-Dichlorophenyl)prop-2-enoyl]-2-methoxybenzene-1-sulfonamide (**4i**).* White crystals; 66% yield; m.p.: 245−247 °C. ^{1}H NMR (400 MHz, DMSO-d_6) δ ppm: 4.05 (s, 3H, 4-OCH_3 of benzene sulfonamide ring), 7.31 (s, 2H, SO_2NH_2), 7.39 (d, 1H, J = 8.0, 3-H of benzene sulfonamide ring), 7.74 (d, 1H, J = 16.0, COCH═C**H**), 7.75 (d, 1H, J = 8.0, 5-H of dihalophenyl ring), 7.92 (d, 1H, J = 8.0, 2-H of dihalophenyl ring), 8.09 (d, 1H, J = 16.0, COC**H**═CH), 8.32 (s, 1H, 6-H of dihalophenyl ring), 8.47 (s, 1H, 6-H of benzene sulfonamide ring), 8.55 (d, 1H, J = 8.0, 4-H of benzene sulfonamide ring). ^{13}C NMR (101 MHz, DMSO-d_6) δ ppm: 57.27, 113.08, 124.04, 128.85, 129.58, 130.98, 131.36, 131.71, 132.28, 133.26, 135.47, 136.00, 136.91, 141.76, 160.31, and 187.18. MS (ESI) (m/z): 385.33 $[M + 1]^+$, 387.34 $[M + 3]^+$. Anal. calcd. for $C_{16}H_{13}Cl_2NO_4S$: C, 49.76; H, 3.39; N, 3.63; S, 8.30. Found: C, 49.97; H, 3.58; N, 3.81; S, 8.59.

*7.1.3.10. 2-Methoxy-5-[(2E)-3-(naphthalen-1-yl)prop-2-enoyl]benzene-1-sulfonamide (**4j**).* Yellow powder; 79% yield; m.p.: 178−179 °C. ^{1}H NMR (400 MHz, DMSO-d_6) δ ppm: 4.06 (s, 3H, 4-OCH_3 of benzene sulfonamide ring), 7.35 (s, 2H, SO_2NH_2), 7.39 (d,1H, J = 8.0, 3-H of benzene sulfonamide ring), 7.59−7.68 (m, 3H, 3,6,7-H_3 of naphthyl ring), 8.01−8.09 (m, 3H, COCH═C**H** and 2,4-H_2 of naphthyl ring), 8.27 (d, 1H, J = 8.0, 4-H of benzene sulfonamide ring), 8.30 (d, 1H, J = 8.0, 5-H of naphthyl ring), 8.53 (s, 1H, 6-H of benzene sulfonamide ring), 8.57 (d, 1H, J = 8.0, 8-H of naphthyl ring), 8.60 (d, 1H, J = 16.0, COC**H**═CH). ^{13}C NMR (101 MHz, DMSO-d_6) δ ppm: 57.23, 113.17, 123.45, 124.41, 126.20 (2C), 126.84, 127.78, 128.77, 129.29, 129.76, 131.43, 131.66, 131.69, 132.19, 133.83, 135.34, 140.50, 160.22, and 187.35. MS (ESI) (m/z): 367.17 $[M^+]$. Anal. calcd. for $C_{20}H_{17}NO_4S$: C, 65.38; H, 4.66; N, 3.81; S, 8.73. Found: C, 65.23; H, 4.79; N, 3.98; S, 8.59.

*7.1.3.11. 2-Methoxy-5-[(2E)-3-(Naphthalen-2-Yl)Prop-2-Enoyl]Benzene-1-Sulfonamide (**4 K**).* Yellow crystals; 70% yield; m.p.: 214−246 °C. ^{1}H NMR (400 MHz, DMSO-d_6) δ ppm: 4.06 (s, 3H, 4-OCH_3 of benzene sulfonamide ring), 7.33−7.40 (m, 3H, SO_2NH_2 + 3-H of benzene sulfonamide ring), 7.61 (m, 2H, 3,6-H_2 of naphthyl ring), 8.00−8.15 (m, 6H, COCH═C**H** + 1,4-H_2 of naphthyl ring + 4-H of benzene sulfonamide ring + 5-H of naphthyl ring), 8.38−8.57 (m, 3H, 6-H of benzene sulfonamide ring + 8-H of naphthyl ring + COC**H**═CH). ^{13}C NMR (101 MHz, DMSO-d_6) δ ppm: 57.23, 113.18, 122.12, 124.73, 127.39, 128.11, 128.20, 128.65, 129.09 (2C), 129.80, 131.33, 131.99, 132.62, 133.39, 134.42135.38, 144.76, 160.18, and 187.54. MS (ESI) (m/z): 367.18 $[M^+]$. Anal. calcd. for $C_{20}H_{17}NO_4S$: C, 65.38; H, 4.66; N, 3.81; S, 8.73. Found: C, 65.41; H, 4.82; N, 4.05; S, 8.61.

*7.1.3.12. 5-[(2E)-3-(6-Bromo-2H-1,3-benzodioxol-5-yl)-prop-2-enoyl]-2-methoxybenzene-1-sulfonamide (**4l**).* Yellow crystals; 55% yield; m.p.: 253−255 °C. ^{1}H NMR (400 MHz, DMSO-d_6) δ ppm: 4.05 (s, 3H, 4-OCH_3 of benzene sulfonamide ring), 6.19 (s, 2H, OCH_2O), 7.29 (s, 2H, SO_2NH_2), 7.37 (s, 1H, 5-H, Ar-H), 7.38 (d, 1H, J = 8.0, 3-H of benzene sulfonamide ring), 7.90 (d, 1H, J = 16.0, COCH═

https://doi.org/10.1021/acsomega.2c07285
ACS Omega 2023, 8, 7666−7683

CH), 7.91 (s, 1H, 1-H, Ar-H), 7.99 (d, 1H, J = 16.0, COCH=CH), 8.47 (ds, 1H, J = 4.0, 6-H of benzene sulfonamide ring), 8.53 (d, 1H, J = 8.0, 4-H of benzene sulfonamide ring). ^{13}C NMR (101 MHz, DMSO-d_6) δ ppm: 57.24, 103.19, 107.73, 113.04, 113.31, 118.89, 122.67, 127.70, 128.72, 129.74, 132.24, 135.36, 141.91, 148.47, 150.90, 160.21, and 187.04. MS (ESI) (m/z): 439.53 $[M + 1]^+$, 442.22 $[M + 3]^+$. Anal. calcd. for $C_{17}H_{14}BrNO_6S$: C, 46.38; H, 3.21; N, 3.18; S, 7.28. Found: C, 46.24; H, 3.39; N, 3.29; S, 7.39.

*7.1.3.13. 5-[(2E)-3-(2,2-Difluoro-2H-1,3-benzodioxol-5-yl)-prop-2-enoyl]-2-methoxybenzene-1-sulfonamide (**4m**).* Brown powder; 86% yield; m.p.: 206−208 °C. ^{1}H NMR (400 MHz, DMSO-d_6) δ ppm: 4.05 (s, 3H, 4-OCH_3 of benzene sulfonamide ring), 7.31−7.35 (m, 3H, SO_2NH_2 + 3-H of benzene sulfonamide ring), 7.42 (d, 1H, 3-H, J = 8.0, of Ar-H), 7.52 (d, 1H, 4-H, J = 8.0, of Ar-H), 7.71 (d, 1H, J = 16.0, COCH=CH), 7.79 (d, 1H, J = 8.0, 3-H of benzene sulfonamide ring), 7.96 (d, 1H, J = 16.0, COCH=CH), 8.42−8.44 (m, 2H, 4,6-H_2 of benzene sulfonamide ring). ^{13}C NMR (101 MHz, DMSO-d_6) δ ppm: 57.27, 112.22, 113.36, 118.87, 125.13, 125.28, 125.83, 128.74, 129.31, 131.61, 132.28, 135.25, 135.39, 141.80, 143.59, 160.41, and 186.97. MS (ESI) (m/z): 397.76 $[M^+]$. Anal. calcd. for $C_{17}H_{13}F_2NO_6S$: C, 51.39; H, 3.30; N, 3.53; S, 8.07. Found: C, 51.57; H, 3.43; N, 3.71; S, 8.21.

*7.1.3.14. 5-[(2E)-3-(2,3-Dihydro-1,4-benzodioxin-6-yl)-prop-2-enoyl]-2-methoxybenzene-1-sulfonamide (**4n**).* Yellow crystals; 78% yield; m.p.: 196−198 °C. ^{1}H NMR (400 MHz, DMSO-d_6) δ ppm: 4.04 (s, 3H, 4-OCH_3 of benzene sulfonamide ring), 4.32 (d, 2H, J = 4.0, OCH_2CH_2O), 6.95 (d, 1H, J = 8.0, 3-H of benzene sulfonamide ring), 7.29−7.41 (m, 11H, SO_2NH_2 + Ar-H), 7.53 (s, 1H, Ar-H), 7.68 (d, 1H, J = 16.0, COCH=CH), 7.82 (d, 1H, J = 16.0, COCH=CH), 8.21 (d, 2H, J = 8.0, Ar-H), 8.30 (s, 2H, 2-H of Ar-H), 8.44 (ds, 1H, J = 4.0, 6-H of benzene sulfonamide ring), 8.51 (dd, 1H, J = 4.0, J = 8.0, 4-H of benzene sulfonamide ring). ^{13}C NMR (101 MHz, DMSO-d_6) δ ppm: 57.28, 113.17, 124.75, 127.41, 128.21, 128.79, 129.13, 129.52, 130.54, 132.29, 132.69, 134.86, 135.44, 139.04, 160.35, and 187.18. MS (ESI) (m/z): 375.14 $[M^+]$. Anal. calcd. for $C_{18}H_{17}NO_6S$: C, 57.59; H, 4.56; N, 3.73; S, 8.54. Found: C, 57.81; H, 4.70; N, 3.99; S, 8.60.

*7.1.3.15. 2-Methoxy-5-[(2E)-3-(pyridin-3-yl)prop-2-enoyl]-benzene-1-sulfonamide (**4o**).* Brown powder; 65% yield; m.p.: 198−200 °C. ^{1}H NMR (400 MHz, DMSO-d_6) δ ppm: 4.05 (s, 3H, 4-OCH_3 of benzene sulfonamide ring), 7.32 (s, 2H, SO_2NH_2), 7.40 (d, 1H, J = 8.0, 3-H of benzene sulfonamide ring), 5.51−5.54 (d, 1H, J = 8.0, 5-H of pyridine ring), 7.81 (d, 1H, J = 16.0, COCH=CH), 8.12 (d, 1H, J = 16.0, COCH=CH), 8.39 (d, 1H, 6-H, J = 8.0, 4-H of benzene sulfonamide ring), 8.48 (s, 1H, 6-H of benzene sulfonamide ring), 8.54 (d, 1H, J = 8.0, 6-H of pyridine ring), 8.64 (d, 1H, J = 8.0, 4-H of pyridine ring), 9.06 (s, 1H, 2-H of pyridine ring). ^{13}C NMR (101 MHz, DMSO-d_6) δ ppm: 57.26, 113.15, 123.86, 124.48, 128.74, 129.55, 130.95, 132.04, 135.44, 136.29, 141.13, 150.82, 151.53, 160.30, and 187.20. MS (ESI) (m/z): 317.79 $[M^+]$. Anal. calcd. for $C_{15}H_{14}N_2O_4S$: C, 56.59; H, 4.43; N, 8.80; S, 10.07. Found: C, 56.78; H, 4.60; N, 9.04; S, 10.04.

7.2. NCI-60 Screening of Compounds. Compounds **4a**−**4o** were submitted for anticancer activity screening against 60 different cell lines, representing nine different human tissues, by the Developmental Therapeutics Program of the United States National Cancer Institute, Bethesda, MD.[29] The NCI-60 screen was done by employing the SRB assay. The results provided are growth percentages relative to the no-drug control and relative to the time zero number of cells. Values of percentage growth inhibition (% GI) were calculated from the values of mean growth percentages as (100 − growth %). The compounds that met certain criteria defined by the DTP NCI were promoted to the five-dose screening stage by the NCI to assess the dose−response curves in the 60-cell line panel. Five 10-fold serial dilutions (100, 10, 1.0, 0.1, and 0.01 μM) for each derivative were tested against each cell line to assess growth percentage following treatment for 48 h. Different parameters were determined from the dose−response relationship. The values of GI_{50}, TGI, and LC_{50} parameters were computed using GraphPad Prism 9.0.

7.3. Carbonic Anhydrase Inhibitory Activity. The inhibition of catalytic activities of recombinant hCA isoforms I, II, IX, and XII by compounds **3** and **4a**−**4o** was measured using an Applied Photophysics stopped-flow instrument.[53] The catalysis of carbon dioxide hydration reactions was performed in 20 mM HEPES buffer (pH 7.5) and 20 mM Na_2SO_4 to maintain constant the ionic strength. Initial rates of hCA-catalyzed CO_2 hydration reaction were followed for 10−100 s using phenol red (0.2 mM) as an indicator, measuring the absorbance at λ_{max} of 557 nm. The CO_2 concentrations used to determine the kinetic parameters and inhibition constants ranged from 1.7 to 17 mM. The beginning velocity for each inhibitor was determined based on the first 5−10% of the reaction. The uncatalyzed reaction rates were deduced from the total measured rates. Stock inhibitor solutions (0.1 mM) were prepared followed by serial dilutions with the assay buffer down to 0.01 nM. The inhibitor and enzyme solutions were pre-incubated for 15 min at room temperature to allow for the formation of the enzyme−inhibitor complex. The inhibition constants were calculated using non-linear least-squares methods using the ChengPrusoff equation in PRISM 3. Each inhibition constant value represents the average of at least three independent measurements.

7.4. Pim-1 Kinase Inhibitory Activity. The *in vitro* Pim-1 kinase inhibitory activity of the selected compounds was assessed using the Promega ADP-Glo kinase assay according to the manufacturer's protocol.[54] The ADP formed from the kinase reaction is converted into ATP, which is converted into light by Ultra-Glo Luciferase. The luminescence signal positively correlates with the remaining kinase activity. Five-point measurements were obtained for each compound: 100, 10, 1, and 0.1 μM. The luminescence signal was measured on a Tecan Spark microplate reader.[55] The statistical data analysis and IC_{50} values were determined using GraphPad Prism 9.0.

7.5. Reactive Oxygen Species (ROS) Level. A reactive oxygen species fluorometric assay kit (Elab Science, Catalog No: E-BC-K138-F) was used to detect the cellular ROS level following the manufacturer's protocol. After pretreatment of HCT116 cells with H_2O_2 and either **4j** (2.94 μM) or DMSO control, DCFH-DA was incubated with the cells for 20 min at 37 °C. Fluorescence intensity was recorded at an excitation wavelength of 502 nm and the emission wavelength of 530 nm using a BD FACSCalibur flow cytometer.

7.6. Nrf2 Activation and ROS Measurement. HCT116 cells were treated with either 2.94 μM **4j** or DMSO vehicle control. The nuclear protein was harvested from the cells with the Nuclear Extraction Kit (ab113474, Abcam) and detected with BCA kits (Thermo Fisher). The Nrf2 activation was detected using the nuclear protein with the Colorimetric Nrf2 Transcription Factor Assay Kit (ab207223, Abcam, Cambridge, UK) with an ROBONIK P2000 microplate ELISA reader at 450 nm following the kit manufacturer's protocol. A standard curve

https://doi.org/10.1021/acsomega.2c07285
ACS Omega 2023, 8, 7666−7683

of Nrf2 was plotted, and the Nrf2 sample concentration was interpolated from a standard curve relating the intensity of the color (O.D.) to the concentration of standards.

7.6.1. Cell Lines, Culture Conditions, and MTT Assay. HCT116 cells (ATCC: CCL-247), LOX IMVI cells (ATCC: CVCL 1381), U251 cells (ATCC: HTB-17), and HEK293T cell line (ATCC: CRL-3216) were obtained from the American Type Culture Collection and maintained at the Cell Culture Holding Company for Biological Products and Vaccines Department (Vacsera), Dokki-Giza, Egypt. Cells were cultured in Dulbecco's modified Eagle medium supplemented with 10% fetal bovine serum (Sigma-Aldrich, USA), 1% of penicillin/streptomycin (Gibco, USA), 10 μg/mL insulin (Sigma-Aldrich, USA), and 2 mM L-glutamine (Lonza Verviers Sprl, Belgium) and incubated at 37 °C in 5% CO_2. For the MTT assay, cells were seeded at a density of 1.2−1.8 × 10^5 cells/well in a volume of 100 μL per well into 96-well cell culture plates and incubated for 24 h prior to treatment. MTT assays were conducted for **4d** and **4j** to detect their potential cytotoxicity and determine the half maximal inhibitory concentration (IC_{50}). Cells were incubated for 48 h with five serial dilutions (100, 25, 6.25, 1.56, and 0.4 μM) of each compound, each as a single treatment in triplicate, compared to the negative control group (drug free media) and untreated cell control. The media were discarded at the end of the 48 hhour incubation period, 20 μL of 3-[4,5-dimethylthiazol-2-yl]-2,5-diphenyl-tetrazolium bromide (MTT) (Sigma-Aldrich, USA) (5 mg/mL) solution in phosphate-buffered saline (PBS) (Lonza Verviers Sprl, Belgium) was added to each plate, and the supernatants were then removed with care. The formazan crystals were dissolved in 100 μL of DMSO (Sigma-Aldrich, USA) and measured at 450 nm using an ELISA microplate reader (Bioline Eliza Reader, India). Each concentration was tested three times. The percentage of viable cells was calculated according to the formula 100 × (As − Ab)/(Ac − Ab), where As is the absorbance of cells treated with compound, Ab = no cells (blank) absorbance, and Ac = absorbance of DMSO-control treated cells. The statistical data analysis and IC_{50} values were determined using GraphPad Prism 9.0.

7.7. Cell Cycle and Apoptosis Analysis. To determine the effect of **4j** on the cell cycle status in HCT116 cells, the commercial Abcam Propidium Iodide Flow Cytometry Kit (ab139418) was used to measure the DNA content. HCT116 cell cultures were treated with either the DMSO control or 2.94 μM **4j**. The cells were harvested in a single cell suspension, fixed in 66% ethanol, and kept at 4 °C for 2 h. The cells were rehydrated cells in PBS and stained with propidium iodide and RNAse for 30 min. Propidium iodide (PI) fluorescence intensity was determined on FL2 of the BD FACSCalibur flow cytometer and 488 nM laser excitation. [λ_{max} excitation = 493 nm; λ_{max} emission = 636 nm].

Membrane phosphatidylserine translocates from the inner face of the plasma membrane to the cell surface once apoptosis is initiated. Extrinsic and intrinsic apoptosis in HCT116 induced by **4j** was detected by staining with a fluorescent conjugate of Annexin V. The cells were treated with **4j** at 2.94 μM for 24 h. The commercial BioVision Annexin V-FITC Apoptosis Detection Kit (BD Biosciences, USA) was used. The assay was performed following manufacturer's instructions. Annexin V-FITC binding fluorescence detection was done on FL1 of the BD FACSCalibur flow cytometer [λ_{max} excitation = 488 nm; λ_{max} emission = 530 nm]. Both Annexin V-FITC and PI staining were performed to differentiate between apoptosis and necrosis.

7.8. *In Silico* Studies. *7.8.1. In Silico Physicochemical Properties and ADME Prediction.* Molecular structures of the compounds were converted into SMILES using ChemDraw 12.0. The SMILES were used as an input in the web-based Swiss-ADME tool, http://www.Swissadme.ch/index.php, to calculate the physicochemical descriptors to evaluate pharmacokinetics and drug-likeness and medicinal chemistry friendliness.[38] Furthermore, the Swiss-ADME tool was used for prediction of permeability through the human gastrointestinal tract and blood−brain barrier.

7.8.2. Molecular Docking Simulation. Molecular docking simulation studies were performed using Molecular Operating Environment software (MOE ver.2020, Chemical Computing Group Inc., Montreal, Canada).[56] The three-dimensional X-ray crystal structure of CA IX was retrieved from the Protein Data Bank (PDB ID: 5FL4).[41] The structure of Pim-1 kinase in complex with an inhibitor at 2.5 Å resolution (PDB ID: 2OBJ) was retrieved from the Protein Data Bank.[57] Cocrystallized water molecules were retained as some are involved in key ligand interactions. The protein structure was prepared, and protonation was adjusted using the Protonate 3D module at 277° K and pH 7.4. Partial charges were assigned using Merck Molecular Force Field 94× (MMFF94X),[58] and hydrogen atoms were minimized. The ligand-binding site was used as a search space for potential docking poses. The bound ligand was redocked into the enzyme binding site to guarantee reliability of the docking protocol (RMSD < 2 Å) to give reproducible results. The triangle matcher placement method was employed. The docked poses were scored by the London dG scoring function. Visualization of 2D interactions and generation of 2D ligand−receptor interaction figures was done using Biovia Discovery Studio Visualizer 2021.[59]

■ ASSOCIATED CONTENT

Supporting Information

The Supporting Information is available free of charge at https://pubs.acs.org/doi/10.1021/acsomega.2c07285.

Spectral Data of compounds **4a-4o**: ^{1}H NMR and ^{13}C NMR spectra; NCI-DTP screening results: single dose mean graphs for **4a-4o** and Dose−response curves for **4b-4l**, and **4o**; Dose−response curves for **3**, **4d**, and **4j** against hCA I, II, IX and XII; *In silico* Swiss target prediction for **4a-4o**.

■ AUTHOR INFORMATION

Corresponding Authors

Shaimaa M. Aboukhatwa − *Department of Pharmaceutical Chemistry, Faculty of Pharmacy, Tanta University, Tanta 31527, Egypt;* Present Address: Department of Pharmaceutical Sciences, College of Pharmacy, University of Illinois at Chicago, Chicago, IL 60608; orcid.org/0000-0002-5013-7158; Email: shaymaa.aboukhatwa@pharm.tanta.edu.eg

Claudiu T. Supuran − *Department of Neurofarba, Section of Pharmaceutical and Nutraceutical Sciences, University of Florence, 50019 Sesto Fiorentino, Firenze, Italy;* orcid.org/0000-0003-4262-0323; Email: claudiu.supuran@unifi.it

Authors

Peter A. Sidhom − *Department of Pharmaceutical Chemistry, Faculty of Pharmacy, Tanta University, Tanta 31527, Egypt;* orcid.org/0000-0003-2579-6351

https://doi.org/10.1021/acsomega.2c07285
ACS Omega 2023, 8, 7666−7683

Andrea Angeli − *Department of Neurofarba, Section of Pharmaceutical and Nutraceutical Sciences, University of Florence, 50019 Sesto Fiorentino, Firenze, Italy;* orcid.org/0000-0002-1470-7192

Haytham O. Tawfik − *Department of Pharmaceutical Chemistry, Faculty of Pharmacy, Tanta University, Tanta 31527, Egypt;* orcid.org/0000-0001-6455-5716

Complete contact information is available at: https://pubs.acs.org/10.1021/acsomega.2c07285

Notes

The authors declare no competing financial interest.

■ ACKNOWLEDGMENTS

The authors acknowledge the National Cancer Institute Development Therapeutics Program (NCI-DTP) for providing screening results against the cancer cell line panel.

■ REFERENCES

(1) Zhuang, C.; Zhang, W.; Sheng, C.; Zhang, W.; Xing, C.; Miao, Z. Chalcone: A Privileged Structure in Medicinal Chemistry. *Chem. Rev.* **2017**, *117*, 7762−7810.

(2) Elkanzi, N. A. A.; Hrichi, H.; Alolayan, R. A.; Derafa, W.; Zahou, F. M.; Bakr, R. B. Synthesis of Chalcones Derivatives and Their Biological Activities: A Review. *ACS Omega* **2022**, *7*, 27769−27786.

(3) Zhou, B.; Xing, C. Diverse Molecular Targets for Chalcones with Varied Bioactivities. *Med. Chem.* **2015**, *5*, 388−404.

(4) (a) Okolo, E. N.; Ugwu, D. I.; Ezema, B. E.; Ndefo, J. C.; Eze, F. U.; Ezema, C. G.; Ezugwu, J. A.; Ujam, O. T. New chalcone derivatives as potential antimicrobial and antioxidant agent. *Sci. Rep.* **2021**, *11*, 21781. (b) Perez-Gonzalez, A.; Castaneda-Arriaga, R.; Guzman-Lopez, E. G.; Hernandez-Ayala, L. F.; Galano, A. Chalcone Derivatives with a High Potential as Multifunctional Antioxidant Neuroprotectors. *ACS Omega* **2022**, *7*, 38254−38268.

(5) (a) Rehuman, N. A.; Oh, J. M.; Nath, L. R.; Khames, A.; Abdelgawad, M. A.; Gambacorta, N.; Nicolotti, O.; Jat, R. K.; Kim, H.; Mathew, B. Halogenated Coumarin-Chalcones as Multifunctional Monoamine Oxidase-B and Butyrylcholinesterase Inhibitors. *ACS Omega* **2021**, *6*, 28182−28193. (b) Noser, A. A.; Shehadi, I. A.; Abdelmonsef, A. H.; Salem, M. M. Newly Synthesized Pyrazolinone Chalcones as Anticancer Agents via Inhibiting the PI3K/Akt/ERK1/2 Signaling Pathway. *ACS Omega* **2022**, *7*, 25265−25277.

(6) Go, M. L.; Wu, X.; Liu, X. L. Chalcones: an update on cytotoxic and chemoprotective properties. *Curr. Med. Chem.* **2005**, *12*, 481−499.

(7) Gomes, M. N.; Muratov, E. N.; Pereira, M.; Peixoto, J. C.; Rosseto, L. P.; Cravo, P. V. L.; Andrade, C. H.; Neves, B. J. Chalcone Derivatives: Promising Starting Points for Drug Design. *Molecules* **2017**, *22*, 1210.

(8) Jackson, P. A.; Widen, J. C.; Harki, D. A.; Brummond, K. M. Covalent Modifiers: A Chemical Perspective on the Reactivity of α,β-Unsaturated Carbonyls with Thiols via Hetero-Michael Addition Reactions. *J. Med. Chem.* **2017**, *60*, 839−885.

(9) Higuchi, K.; Watanabe, T.; Tanigawa, T.; Tominaga, K.; Fujiwara, Y.; Arakawa, T. Sofalcone, a gastroprotective drug, promotes gastric ulcer healing following eradication therapy for Helicobacter pylori: a randomized controlled comparative trial with cimetidine, an H2-receptor antagonist. *J. Gastroenterol. Hepatol.* **2010**, *25*, S155−S160.

(10) Baell, J. B.; Holloway, G. A. New substructure filters for removal of pan assay interference compounds (PAINS) from screening libraries and for their exclusion in bioassays. *J. Med. Chem.* **2010**, *53*, 2719−2740.

(11) (a) Capuzzi, S. J.; Muratov, E. N.; Tropsha, A. Phantom PAINS: Problems with the Utility of Alerts for Pan-Assay INterference CompoundS. *J. Chem. Inf. Model.* **2017**, *57*, 417−427. (b) Lagorce, D.; Oliveira, N.; Miteva, M. A.; Villoutreix, B. O. Pan-assay interference compounds (PAINS) that may not be too painful for chemical biology projects. *Drug Discovery Today* **2017**, *22*, 1131−1133.

(12) Sutanto, F.; Konstantinidou, M.; Dömling, A. Covalent inhibitors: a rational approach to drug discovery. *RSC Med. Chem.* **2020**, *11*, 876−884.

(13) de Freitas Silva, M.; Pruccoli, L.; Morroni, F.; Sita, G.; Seghetti, F.; Viegas, C.; Tarozzi, A. The Keap1/Nrf2-ARE Pathway as a Pharmacological Target for Chalcones. *Molecules* **2018**, *23*, 1803.

(14) Kumar, V.; Kumar, S.; Hassan, M.; Wu, H.; Thimmulappa, R. K.; Kumar, A.; Sharma, S. K.; Parmar, V. S.; Biswal, S.; Malhotra, S. V. Novel chalcone derivatives as potent Nrf2 activators in mice and human lung epithelial cells. *J. Med. Chem.* **2011**, *54*, 4147−4159.

(15) Kim, W.; Lee, H.; Kim, S.; Joo, S.; Jeong, S.; Yoo, J. W.; Jung, Y. Sofalcone, a gastroprotective drug, covalently binds to KEAP1 to activate Nrf2 resulting in anti-colitic activity. *Eur. J. Pharmacol.* **2019**, *865*, No. 172722.

(16) Wu, S.; Lu, H.; Bai, Y. Nrf2 in cancers: A double-edged sword. *Cancer Med.* **2019**, *8*, 2252−2267.

(17) Wang, C.; Wu, P.; Shen, X.-L.; Wei, X.-Y.; Jiang, Z.-H. Synthesis, cytotoxic activity and drug combination study of tertiary amine derivatives of 2′,4′-dihydroxyl-6′-methoxyl-3′,5′-dimethylchalcone. *RSC Adv.* **2017**, *7*, 48031−48038.

(18) Kipp, A. P.; Deubel, S.; Arner, E. S. J.; Johansson, K. Time- and cell-resolved dynamics of redox-sensitive Nrf2, HIF and NF-kappaB activities in 3D spheroids enriched for cancer stem cells. *Redox Biol.* **2017**, *12*, 403−409.

(19) (a) Chrastina, A.; Závada, J.; Parkkila, S.; Kaluz, Š.; Kaluzová, M.; Rajcani, J.; Pastorek, J.; Pastoreková, S. Biodistribution and pharmacokinetics of 125I-labeled monoclonal antibody M75 specific for carbonic anhydrase IX, an intrinsic marker of hypoxia, in nude mice xenografted with human colorectal carcinoma. *Int. J. Cancer* **2003**, *105*, 873−881. (b) Rafajová, M.; Zatovicová, M.; Kettmann, R.; Pastorek, J.; Pastoreková, S. Induction by hypoxia combined with low glucose or low bicarbonate and high posttranslational stability upon reoxygenation contribute to carbonic anhydrase IX expression in cancer cells. *Int. J. Oncol.* **2004**, *24*, 995−1004.

(20) (a) Ivanov, S.; Liao, S. Y.; Ivanova, A.; Danilkovitch-Miagkova, A.; Tarasova, N.; Weirich, G.; Merrill, M. J.; Proescholdt, M. A.; Oldfield, E. H.; Lee, J.; et al. Expression of hypoxia-inducible cell-surface transmembrane carbonic anhydrases in human cancer. *Am. J. Pathol.* **2001**, *158*, 905−919. (b) Hussain, S. A.; Ganesan, R.; Reynolds, G.; Gross, L.; Stevens, A.; Pastorek, J.; Murray, P. G.; Perunovic, B.; Anwar, M. S.; Billingham, L.; James, N. D.; Spooner, D.; Poole, C. J.; Rea, D. W.; Palmer, D. H. Hypoxia-regulated carbonic anhydrase IX expression is associated with poor survival in patients with invasive breast cancer. *Br. J. Cancer* **2007**, *96*, 104−109. (c) Swinson, D. E. B.; Jones, J. L.; Richardson, D.; Wykoff, C.; Turley, H.; Pastorek, J.; Taub, N.; Harris, A. L.; O'Byrne, K. J. Carbonic anhydrase IX expression, a novel surrogate marker of tumor hypoxia, is associated with a poor prognosis in non-small-cell lung cancer. *J. Clin. Oncol.* **2003**, *21*, 473−482. (d) Ilardi, G.; Zambrano, N.; Merolla, F.; Siano, M.; Varricchio, S.; Vecchione, M.; De Rosa, G.; Mascolo, M.; Staibano, S. Histopathological determinants of tumor resistance: a special look to the immunohistochemical expression of carbonic anhydrase IX in human cancers. *Curr. Med. Chem.* **2014**, *21*, 1569−1582.

(21) (a) Haapasalo, J. A.; Nordfors, K. M.; Hilvo, M.; Rantala, I. J.; Soini, Y.; Parkkila, A. K.; Pastorekova, S.; Pastorek, J.; Parkkila, S. M.; Haapasalo, H. K. Expression of carbonic anhydrase IX in astrocytic tumors predicts poor prognosis. *Clin. Cancer Res.* **2006**, *12*, 473−477. (b) Giatromanolaki, A.; Koukourakis, M. I.; Sivridis, E.; Pastorek, J.; Wykoff, C. C.; Gatter, K. C.; Harris, A. L. Expression of hypoxia-inducible carbonic anhydrase-9 relates to angiogenic pathways and independently to poor outcome in non-small cell lung cancer. *Cancer Res.* **2001**, *61*, 7992−7998. (c) Chia, S. K.; Wykoff, C. C.; Watson, P. H.; Han, C.; Leek, R. D.; Pastorek, J.; Gatter, K. C.; Ratcliffe, P.; Harris, A. L. Prognostic significance of a novel hypoxia-regulated marker, carbonic anhydrase IX, in invasive breast carcinoma. *J. Clin. Oncol.* **2001**, *19*, 3660−3668.

(22) Lee, K.; Kim, S.; Lee, Y.; Lee, H.; Lee, Y.; Park, H.; Nahm, J. H.; Ahn, S.; Yu, S. J.; Lee, K.; Kim, H. The Clinicopathological and

Prognostic Significance of Nrf2 and Keap1 Expression in Hepatocellular Carcinoma. *Cancer* **2020**, *12*, 2128.
(23) Mokhtari, R. B.; Kumar, S.; Islam, S. S.; Yazdanpanah, M.; Adeli, K.; Cutz, E.; Yeger, H. Combination of carbonic anhydrase inhibitor, acetazolamide, and sulforaphane, reduces the viability and growth of bronchial carcinoid cell lines. *BMC Cancer* **2013**, *13*, 378.
(24) Islam, S. S.; Mokhtari, R. B.; Akbari, P.; Hatina, J.; Yeger, H.; Farhat, W. A. Simultaneous Targeting of Bladder Tumor Growth, Survival, and Epithelial-to-Mesenchymal Transition with a Novel Therapeutic Combination of Acetazolamide (AZ) and Sulforaphane (SFN). *Targeted Oncol.* **2016**, *11*, 209−227.
(25) Su, X.; Jiang, X.; Meng, L.; Dong, X.; Shen, Y.; Xin, Y. Anticancer Activity of Sulforaphane: The Epigenetic Mechanisms and the Nrf2 Signaling Pathway. *Oxid. Med. Cell. Longevity* **2018**, *2018*, 5438179.
(26) Pastorekova, S.; Gillies, R. J. The role of carbonic anhydrase IX in cancer development: links to hypoxia, acidosis, and beyond. *Cancer Metastasis Rev.* **2019**, *38*, 65−77.
(27) (a) Pastorekova, S.; Casini, A.; Scozzafava, A.; Vullo, D.; Pastorek, J.; Supuran, C. T. Carbonic anhydrase inhibitors: the first selective, membrane-impermeant inhibitors targeting the tumor-associated isozyme IX. *Bioorg. Med. Chem. Lett.* **2004**, *14*, 869−873. (b) Abbate, F.; Casini, A.; Owa, T.; Scozzafava, A.; Supuran, C. T. Carbonic anhydrase inhibitors: E7070, a sulfonamide anticancer agent, potently inhibits cytosolic isozymes I and II, and transmembrane, tumor-associated isozyme IX. *Bioorg. Med. Chem. Lett.* **2004**, *14*, 217−223.
(28) Castano, L. F.; Cuartas, V.; Bernal, A.; Insuasty, A.; Guzman, J.; Vidal, O.; Rubio, V.; Puerto, G.; Lukac, P.; Vimberg, V.; et al. New chalcone-sulfonamide hybrids exhibiting anticancer and antituberculosis activity. *Eur. J. Med. Chem.* **2019**, *176*, 50−60.
(29) Shoemaker, R. H. The NCI60 human tumour cell line anticancer drug screen. *Nat. Rev. Cancer* **2006**, *6*, 813−823.
(30) Covell, D. G.; Huang, R.; Wallqvist, A. Anticancer medicines in development: assessment of bioactivity profiles within the National Cancer Institute anticancer screening data. *Mol. Cancer Ther.* **2007**, *6*, 2261−2270.
(31) Skehan, P.; Storeng, R.; Scudiero, D.; Monks, A.; McMahon, J.; Vistica, D.; Warren, J. T.; Bokesch, H.; Kenney, S.; Boyd, M. R. New colorimetric cytotoxicity assay for anticancer-drug screening. *J. Natl. Cancer Inst.* **1990**, *82*, 1107−1112.
(32) Swain, B.; Abhay; Singh, P.; Angeli, A.; Aashritha, K.; Nagesh, N.; Supuran, C. T.; Arifuddin, M. 3-Functionalised benzenesulphonamide based 1,3,4-oxadiazoles as selective carbonic anhydrase XIII inhibitors: Design, synthesis and biological evaluation. *Bioorg. Med. Chem. Lett.* **2021**, *37*, No. 127856.
(33) Daina, A.; Michielin, O.; Zoete, V. SwissTargetPrediction: updated data and new features for efficient prediction of protein targets of small molecules. *Nucleic Acids Res.* **2019**, *47*, W357−W364.
(34) Bachmann, M.; Kosan, C.; Xing, P. X.; Montenarh, M.; Hoffmann, I.; Möröy, T. The oncogenic serine/threonine kinase Pim-1 directly phosphorylates and activates the G2/M specific phosphatase Cdc25C. *Int. J. Biochem. Cell Biol.* **2006**, *38*, 430−443.
(35) Redza-Dutordoir, M.; Averill-Bates, D. A. Activation of apoptosis signalling pathways by reactive oxygen species. *Biochim. Biophys. Acta* **2016**, *1863*, 2977−2992.
(36) Gwak, E. J.; Kim, D.; Hwang, H.-Y.; Kwon, H. J. Mitochondrial ROS Produced in Human Colon Carcinoma Associated with Cell Survival via Autophagy. *Cancer* **2022**, *14*, 1883.
(37) (a) DeNicola, G. M.; Karreth, F. A.; Humpton, T. J.; Gopinathan, A.; Wei, C.; Frese, K.; Mangal, D.; Yu, K. H.; Yeo, C. J.; Calhoun, E. S.; Scrimieri, F.; Winter, J. M.; Hruban, R. H.; Iacobuzio-Donahue, C.; Kern, S. E.; Blair, I. A.; Tuveson, D. A. Oncogene-induced Nrf2 transcription promotes ROS detoxification and tumorigenesis. *Nature* **2011**, *475*, 106−109. (b) Sporn, M. B.; Liby, K. T. NRF2 and cancer: the good, the bad and the importance of context. *Nat. Rev. Cancer* **2012**, *12*, 564−571. (c) Jaramillo, M. C.; Zhang, D. D. The emerging role of the Nrf2-Keap1 signaling pathway in cancer. *Genes Dev.* **2013**, *27*, 2179−2191.
(38) Daina, A.; Michielin, O.; Zoete, V. SwissADME: a free web tool to evaluate pharmacokinetics, drug-likeness and medicinal chemistry friendliness of small molecules. *Sci. Rep.* **2017**, *7*, 42717.
(39) Brenk, R.; Schipani, A.; James, D.; Krasowski, A.; Gilbert, I. H.; Frearson, J.; Wyatt, P. G. Lessons Learnt from Assembling Screening Libraries for Drug Discovery for Neglected Diseases. 2008, 3 (3), 435−444, DOI: 10.1002/cmdc.200700139.
(40) Adkins, C. E.; Mittapalli, R. K.; Manda, V. K.; Nounou, M. I.; Mohammad, A. S.; Terrell, T. B.; Bohn, K. A.; Yasemin, C.; Grothe, T. R.; Lockman, J. A.; Lockman, P. R. P-glycoprotein mediated efflux limits substrate and drug uptake in a preclinical brain metastases of breast cancer model. *Front. Pharmacol.* **2013**, *4*, 136.
(41) Leitans, J.; Kazaks, A.; Balode, A.; Ivanova, J.; Zalubovskis, R.; Supuran, C. T.; Tars, K. Efficient expression and crystallization system of cancer-associated carbonic anhydrase isoform IX. *J. Med. Chem.* **2015**, *58*, 9004−9009.
(42) Le, B. T.; Kumarasiri, M.; Adams, J. R.; Yu, M.; Milne, R.; Sykes, M. J.; Wang, S. Targeting Pim kinases for cancer treatment: opportunities and challenges. *Future Med. Chem.* **2015**, *7*, 35−53.
(43) Muz, B.; de la Puente, P.; Azab, F.; Azab, A. K. The role of hypoxia in cancer progression, angiogenesis, metastasis, and resistance to therapy. *Hypoxia* **2015**, *3*, 83−92.
(44) Emami Nejad, A.; Najafgholian, S.; Rostami, A.; Sistani, A.; Shojaeifar, S.; Esparvarinha, M.; Nedaeinia, R.; Haghjooy Javanmard, S.; Taherian, M.; Ahmadlou, M.; et al. The role of hypoxia in the tumor microenvironment and development of cancer stem cell: a novel approach to developing treatment. *Cancer Cell Int.* **2021**, *21*, 62.
(45) Supuran, C. T. Structure and function of carbonic anhydrases. *Biochem. J.* **2016**, *473*, 2023−2032.
(46) Aspatwar, A.; Tolvanen, M. E.; Parkkila, S. Phylogeny and expression of carbonic anhydrase-related proteins. *BMC Mol. Biol.* **2010**, *11*, 25.
(47) Russo, D.; Varricchio, S.; Ilardi, G.; Martino, F.; Di Crescenzo, R. M.; Pignatiello, S.; Scalvenzi, M.; Costa, C.; Mascolo, M.; Merolla, F.; et al. Tissue Expression of Carbonic Anhydrase IX Correlates to More Aggressive Phenotype of Basal Cell Carcinoma. *Front. Oncol.* **2021**, *11*, No. 659332.
(48) Rajendran, P.; Dashwood, W. M.; Li, L.; Kang, Y.; Kim, E.; Johnson, G.; Fischer, K. A.; Löhr, C. V.; Williams, D. E.; Ho, E.; et al. Nrf2 status affects tumor growth, HDAC3 gene promoter associations, and the response to sulforaphane in the colon. *Clin. Epigenet.* **2015**, *7*, 102.
(49) Torrente, L.; Maan, G.; Oumkaltoum Rezig, A.; Quinn, J.; Jackson, A.; Grilli, A.; Casares, L.; Zhang, Y.; Kulesskiy, E.; Saarela, J.; Bicciato, S.; Edwards, J.; Dinkova-Kostova, A. T.; de la Vega, L. High NRF2 Levels Correlate with Poor Prognosis in Colorectal Cancer Patients and with Sensitivity to the Kinase Inhibitor AT9283 In Vitro. *Biomolecules* **2020**, *10*, 1365.
(50) Bayat Mokhtari, R.; Baluch, N.; Morgatskaya, E.; Kumar, S.; Sparaneo, A.; Muscarella, L. A.; Zhao, S.; Cheng, H. L.; Das, B.; Yeger, H. Human bronchial carcinoid tumor initiating cells are targeted by the combination of acetazolamide and sulforaphane. *BMC Cancer* **2019**, *19*, 864.
(51) Sung, H.; Ferlay, J.; Siegel, R. L.; Laversanne, M.; Soerjomataram, I.; Jemal, A.; Bray, F. Global Cancer Statistics 2020: GLOBOCAN Estimates of Incidence and Mortality Worldwide for 36 Cancers in 185 Countries. *Ca-Cancer J. Clin.* **2021**, *71*, 209−249.
(52) Ferlay, J.; Colombet, M.; Soerjomataram, I.; Parkin, D. M.; Pineros, M.; Znaor, A.; Bray, F. Cancer statistics for the year 2020: An overview. *Int. J. Cancer* **2021**, *149*, 778−789.
(53) Tawfik, H. O.; Petreni, A.; Supuran, C. T.; El-Hamamsy, M. H. Discovery of new carbonic anhydrase IX inhibitors as anticancer agents by toning the hydrophobic and hydrophilic rims of the active site to encounter the dual-tail approach. *Eur. J. Med. Chem.* **2022**, *232*, No. 114190.
(54) Aboukhatwa, S. M.; Ibrahim, A. O.; Aoyama, H.; Al-Behery, A. S.; Shaldam, M. A.; El-Ashmawy, G.; Tawfik, H. O. Nicotinonitrile-derived apoptotic inducers: Design, synthesis, X-ray crystal structure and Pim kinase inhibition. *Bioorg. Chem.* **2022**, *129*, No. 106126.

https://doi.org/10.1021/acsomega.2c07285
ACS Omega 2023, 8, 7666−7683

(55) Zegzouti, H.; Zdanovskaia, M.; Hsiao, K.; Goueli, S. A. ADP-Glo: A Bioluminescent and homogeneous ADP monitoring assay for kinases. *Assay Drug Dev. Technol.* **2009**, *7*, 560−572.
(56) *Molecular Operating Environment (MOE), 2020.09*; 1010 Sherbooke St. West, Suite #910, Chemical Computing Group: Montreal, QC, Canada, H3A 2R7., 2022. (accessed.
(57) Cheney, I. W.; Yan, S.; Appleby, T.; Walker, H.; Vo, T.; Yao, N.; Hamatake, R.; Hong, Z.; Wu, J. Z. Identification and structure-activity relationships of substituted pyridones as inhibitors of Pim-1 kinase. *Bioorg. Med. Chem. Lett.* **2007**, *17*, 1679−1683.
(58) Halgren, T. A. Merck molecular force field. I. Basis, form, scope, parameterization, and performance of MMFF94. *J. Comput. Chem.* **1996**, *17*, 490−519.
(59) *Biovia Discovery Studio Visualizer*; Dassault Systèmes: San Diego, 2021.

https://doi.org/10.1021/acsomega.2c07285
ACS Omega 2023, 8, 7666−7683